Chapter 4: Analyses

Numerical analyses have been performed on selected dams from this study in order to provide a better understanding of the behavior of dams with seepage barriers. The analyses performed include analyses of seepage through the dam and foundation, and deformation of the dam and foundation. The dams analyzed were selected based the quality of subsurface data available to define conditions for analysis, and monitoring data for comparison with the analytical results. Descriptions of the purposes and methodologies for the analyses are provided below.

Analyses have also been performed to investigate the effects of cracks in seepage barriers on the performance of the barrier and the potential for long term deterioration of the barrier. Finite element seepage analyses were performed to investigate the effects of three variables: (1) the aperture of a crack through a seepage barrier, (2) the hydraulic conductivity of the surrounding soil, and (3) the differential head across the barrier, have on the effective hydraulic conductivity of the seepage barrier, have on the velocity of the water seeping through the crack. The methodology and results of these analyses are presented below.

Seepage Analyses on Case Study Dams

Purpose of Seepage Analyses

Seepage analyses were performed to assess the changes that occur in the flow regime due to installation of the seepage barrier. The purpose of these analyses varied depending on the observed behavior of the dam. The following paragraphs summarize properties and issues that were assessed for the various dams.

Effective Hydraulic Conductivity. The effective hydraulic conductivity is defined herein as the seepage barrier hydraulic conductivity value determined by back-analysis. The effective hydraulic conductivity is generally greater than the design hydraulic

conductivity of the barrier infill material (as defined by specification, laboratory testing, or assumed material properties). The differences between effective and design hydraulic conductivity can be attributed to three sources: 1) defects or cracks in the barrier, 2) post-barrier construction changes in the hydraulic conductivity of the soil or bedrock around the barrier, and 3) scale effects. Scale effects were discussed by Britton et al. (2004), who concluded that the measured hydraulic conductivity generally increases with increase in the volume of material tested, as a result of cracks and defects.

Hydraulic Conductivity Ratio. The hydraulic conductivity ratio is the ratio of the effective hydraulic conductivity to the hydraulic conductivity estimated for design.

Head Efficiency. The head efficiency of a seepage barrier has been used by others (Telling et al. 1978a, 1978b, 1978c) to describe the effectiveness of a seepage barrier in reducing hydraulic heads in the downstream portion of a dam, and is defined as the drop in head across the barrier, divided by the total drop in head across the dam.

Exit Gradient Reduction. Seepage barriers are often designed to reduce exit gradients in the downstream portion of the embankment, or in the foundation. The effectiveness of the barrier in reducing exit gradients is assessed by comparing the exit gradients calculated from analyses matching the pre-seepage barrier conditions with values calculated for the post-seepage barrier conditions.

Internal Hydraulic Gradients. The installation of a seepage barrier tends to concentrate the flow of water around the barrier and, as a consequence, increases the hydraulic gradient around the boundaries of the barrier. The increased gradient may initiate mechanisms that affect the performance of the seepage barrier over time. Assessing the location and magnitude of the resulting gradients provides insight into the types of mechanisms that result from barrier installation.

Water Pressures. The installation of a seepage barrier tends to increase water pressure on the upstream side of the barrier and reduce pressures on the downstream side. The

changes in water pressure alters the effective stress within the soil and rock mass, and can lead to changes in volume, changes in shear strength, and changes in hydraulic conductivity. The changes in pressure also concentrate the seepage forces in the dam in the seepage barrier and immediately surrounding soil. These stress changes can lead to post-construction deformation of the seepage barrier, as discussed later in this chapter.

Causes of Long-Term Changes. When the readings from monitoring instrumentation indicate a change in performance of the dam and seepage barrier over time, seepage analyses can be used to assess the changes in the hydraulic conductivities that cause these changes in performance.

Seepage Analyses Methodology

The general procedure for performing these seepage analyses is as follows:

1. Establish a two-dimensional cross section for the analyses and estimate the hydraulic conductivity parameters (including anisotropy) for each zone of the embankment and layer of the foundation. Assess which of the estimates of hydraulic conductivity are most reliable. In many cases this assessment is based on the methods by which the hydraulic conductivities were evaluated. Listed in order from most reliable to least reliable are field piezometer tests (slug tests), laboratory permeability tests, and assessment from grain size or soil/rock description.
2. Perform a seepage back-analysis to refine the less reliable hydraulic conductivity estimates from Step 1. This is done by first analyzing the profile without the seepage barrier in place, using best estimates of hydraulic conductivity and anisotropy. After each run the results of the analyses are compared with measured piezometric data prior to construction of the seepage barrier. The hydraulic conductivity parameters of the soil or rock layers that were deemed the most unreliable in Step 1 are adjusted. The analyses are then rerun with adjusted values of the parameters. This process is repeated until reasonable agreement is reached between the analysis results and the measured values.

3. Perform a second back-analysis on the same profile with the seepage barrier in place, using the final hydraulic conductivity parameters from Step 2 and an estimate of the hydraulic conductivity of the seepage barrier. Compare the results of this analysis with the measured piezometric data after construction of the seepage barrier, and adjust the hydraulic conductivity of the seepage barrier, keeping the hydraulic parameters of the soil and rock layers constant. Repeat this process until reasonable agreement is reached between the analysis results and the measured values. The result of this analysis provides a basis for assessing the effective hydraulic conductivity of the seepage barrier.

These analyses have been performed using the finite element seepage module of the computer program Phase2 by Rocscience (Rocscience 2007).

Deformation Analyses on Case Study Dams

Deformation analyses were performed to assess the potential for cracking of the seepage barrier due to the difference in water pressure between the upstream and downstream sides of the barrier. Cracks in the barrier may affect the efficiency of the barrier and may contribute to long-term changes in the barrier performance. The following paragraphs present summaries of the topics that were assessed for the various dams in the seepage analyses.

Stresses in the Seepage Barrier. The deformation of the barrier will result in bending moments in the barrier. The analyses are used to assess the magnitude of the bending moments and the resulting tensile stresses in the barrier so that the potential for cracking can be assessed.

Potential for Cracking of the Seepage Barrier. The potential for cracking of the barrier was assessed by comparing the calculated stresses with the tensile strength of the barrier infill material. Due to the general lack of tensile strength tests performed on the backfill material, the tensile strength of the concrete, f'_t, was assessed based on the unconfined compressive strength, f'_c, using the following equation (Oluokun 1991):

$$f'_t = 4.5\sqrt{f'_c} \qquad 4\text{-}1$$

where f'_c and f'_t are the unconfined compressive strength and the tensile strength of the concrete in pounds per square inch.

This comparison was performed internally after each stage of the analyses so that the stiffness of the barrier would be reduced when the yield stress was reached. A full description of the procedure is presented in Appendix A.

Location of Cracking. The locations where cracks occur in the seepage barrier are important, because cracks lining up with defects or with highly permeable layers in the dam or foundation may result in higher potential for large flow through the barrier. Details of these mechanisms are presented in Chapter 5.

The procedure for performing the deformation analyses is as follows.

1. Establish a two-dimensional cross section for the analyses and estimate the deformation parameters for each of the zones within the embankment and the foundation. The Duncan and Chang hyperbolic stress-strain relationship (Duncan et. al 1980) was used to model the soil behavior. Hard bedrock was modeled using a linear elastic model.
2. Perform a two-dimensional finite-element deformation analysis to model step-by-step construction of the embankment and filling of the reservoir. The embankment is constructed in six to eight layers (stages) to model the non-linear behavior of soil. The reservoir filling is modeled in one stage using the steady-state groundwater regime calculated in the seepage analyses discussed previously in this chapter.
3. The effects of the seepage barrier are modeled by inserting the barrier in place in one stage (wishing it in place), and analyzing the steady-state seepage condition with the barrier in place. The stress-strain behavior of structural barriers is modeled with a Timoshenko beam element (Rocscience 2007) while soil-bentonite barriers are modeled with two-dimensional elements and Duncan-Chang soil properties.

4. The forces induced by the change in groundwater regime that follows seepage barrier construction are modeled as changes in the seepage and buoyant forces acting within the soil. The change in seepage and buoyant forces due to the seepage barrier are added to the model in the same stage that the seepage barrier is "wished" into place. In order to observe and evaluate the deformations that occur after installation of the seepage barrier, the nodal displacements are reset to zero prior to application of the forces induced by installation of the seepage barrier.

These analyses have been run using the computer program Phase2 by Rocscience (Rocscience 2007).

The Phase2 program does not calculate seepage forces. Therefore, the seepage forces must be calculated outside of the program and inserted into the input files as external loads. Seepage forces are calculated for every node of the finite element mesh where a change in water pressure occurs. A description of the theory, equations, and methods for calculating the seepage forces is presented in Appendix A.

Analyses of Specific Dams

The remainder of this chapter presents descriptions of the analyses performed on specific dams. The dams analyzed were selected based the quality of data available from which to define the seepage and deformation models. Analyses were not performed on dams where there was insufficient data either to define the seepage or deformation parameters of the soils and bedrock, or if there was not sufficient monitoring data with which to compare results.

Upper and Lower Clemson Diversion Dams

Seepage and deformation analyses were performed for Upper and Lower Clemson Diversion Dams. Because of the similarities between the dams and the analyses performed, the analyses are presented together for to allow comparison of the results

from both dams. The seepage analyses were performed to assess the effectiveness of the barriers in reducing the seepage flow beneath the dam, and to provide data on groundwater pressures for use in calculating seepage forces. The deformation analyses were performed to estimate the post-construction deformation of the seepage barriers in order to assess the potential for cracking of the barriers and likely locations of cracks. A generalized cross section representative of both Upper and Lower Clemson Diversion Dams is shown in Figure 4-1. The materials comprising the dams and foundations are described in Chapter 3.

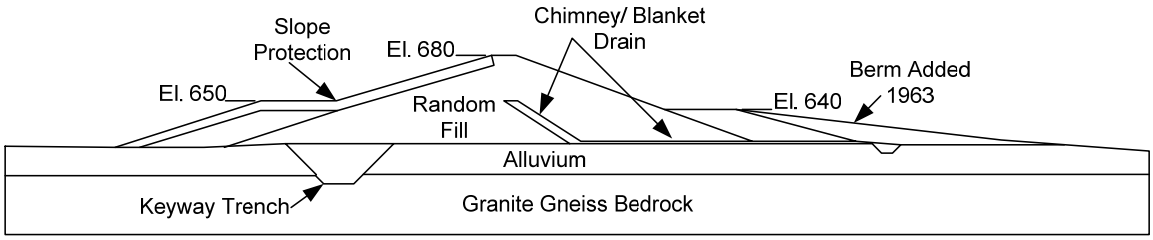

Figure 4-1 Cross section of Upper and Lower Clemson Diversion Dam (modified from USACE 1989, 1983, with permission from USACE)

Seepage Analyses. The dam/foundation systems include four main units: bedrock, alluvium, random fill, and drain material. For the purposes of these analyses the bedrock and the random fill were assumed to have homogeneous hydraulic properties throughout the units. The alluvium was modeled as two units in Clemson Upper Diversion Dam, the upper silt/clay/sand layer and the basal sand and gravel layer. In the Clemson Lower Diversion Dam a third unit consisting of silty sand was included in the alluvium model. The drains were modeled in the seepage analyses using boundary conditions assuming that the hydraulic pressure in the drain materials would be zero. The drain material was grouped into the random fill for the deformation analyses.

Three different cross sections were analyzed for each dam to account for differing conditions in the foundation alluvium that were encountered along the lengths of the dams. The three profiles each for Upper and Lower Clemson Diversion Dams are shown in Figures 4-2 and 4-3, respectively. In the Upper Clemson Diversion Dam cross

sections, Profile UC-AA contains a significant layer of low hydraulic conductivity silt/clay/sand alluvium while Profile UC-BB contains none of this material and Profile UC-CC contains a minor amount. In the Lower Clemson Diversion Dam cross sections, the alluvium in Profile LC-BB consists predominantly of clean sand with no layers of silt, clay or silty sand encountered in the four borings along the profile. The alluvium in Profile LC-CC consists primarily of finer grained soils with a thin layer of clean sand along the base of alluvium. In Profile LC-DD the alluvium consists of silty sand in the upper portion overlying a basal layer of sand and gravel.

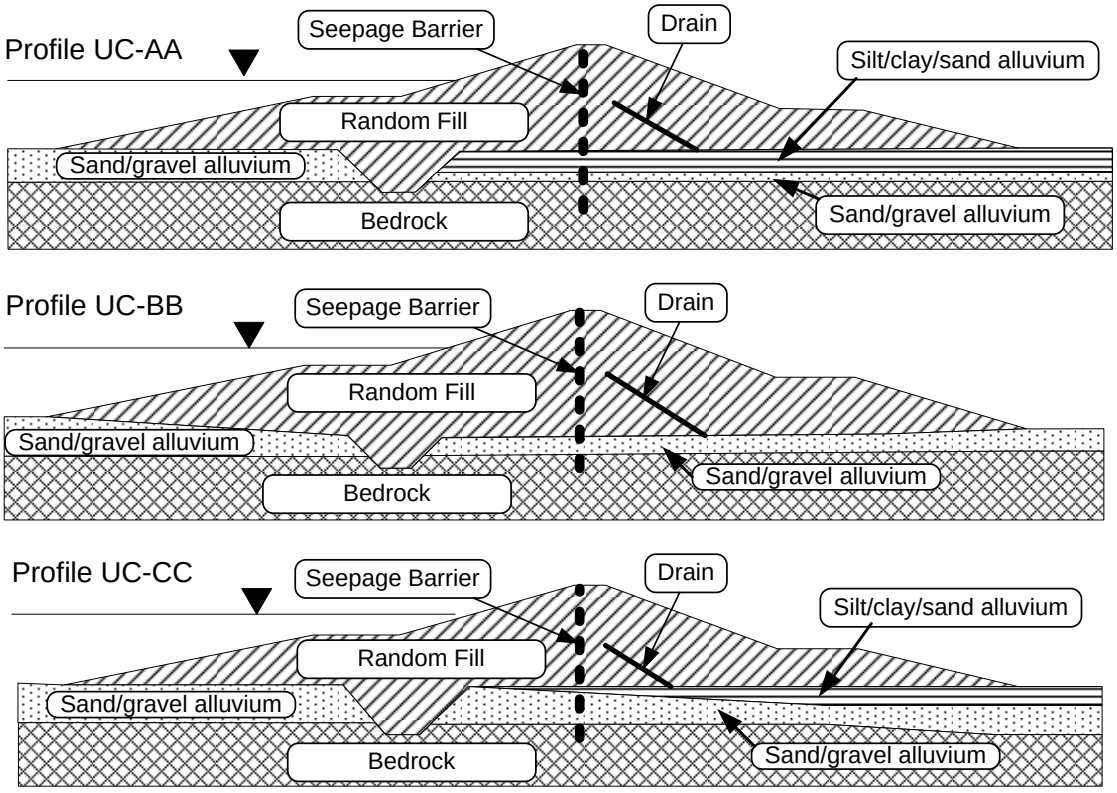

Figure 4-2 Three analysis cross sections for Upper Clemson Diversion Dam

Field pumping tests were performed at both dams to measure the hydraulic conductivity of the basal sand and gravel layers to provide information for design of the seepage barrier. The test at Upper Clemson Diversion Dam resulted in hydraulic conductivity values ranging from 0.03 to 0.09 cm/s, depending on the method of interpretation. Based on these results, a horizontal hydraulic conductivity of 0.05 cm/s was selected for use in the analysis. Two tests performed at Lower Clemson Diversion Dam resulted in hydraulic conductivity values ranging from 0.071 cm/s, where the alluvium consisted of clean sand

(similar to Profile LC-BB), to 0.154 cm/s where the alluvium consisted of silty sand overlying a thin layer of sand and gravel. The values judged to be most representative of the profile being analyzed were used in the analyses. Due to the layered nature of these deposits, vertical to horizontal hydraulic conductivity anisotropy ratios of 0.1 were assumed. The upper silt/clay/sand portion of the alluvium was assumed to have a horizontal hydraulic conductivity of $5x10^{-4}$ cm/s and a vertical to horizontal hydraulic conductivity anisotropy ratio of 0.25. Because the measured value of the basal sand/gravel layer in the alluvium was deemed highly reliable and because it controls the overall behavior of the alluvium, the hydraulic conductivity parameters of the alluvium were kept constant throughout the seepage analyses.

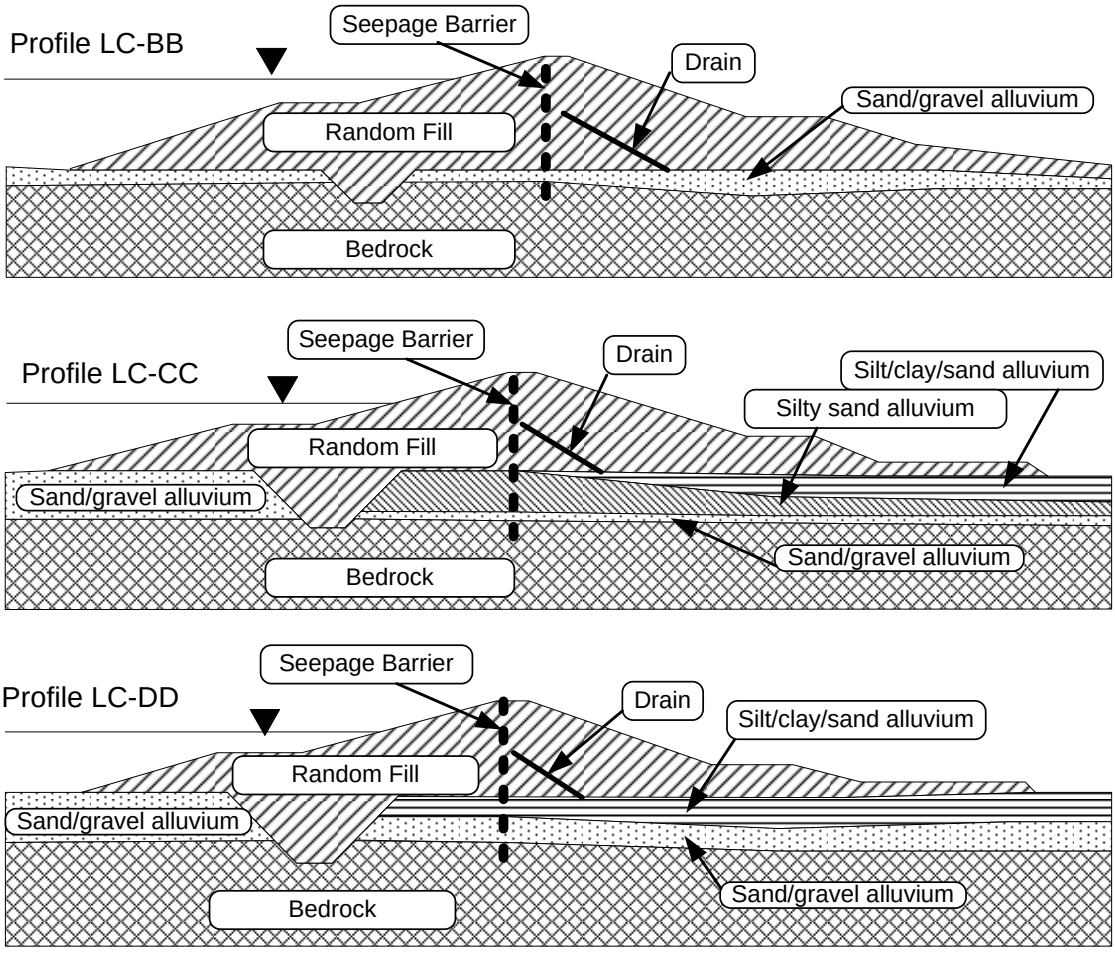

Figure 4-3 Three analysis cross sections for Lower Clemson Diversion Dam

The hydraulic conductivity of the bedrock was measured at both dam sites using piezometer slug tests. The average measured value of horizontal hydraulic conductivity was $3x10^{-4}$ cm/s and the ratio of vertical to horizontal hydraulic conductivity was estimated to be 0.25. These values were also deemed reliable and held constant throughout the seepage analyses.

While holding the hydraulic conductivity parameters for the alluvium and bedrock constant, seepage back-analyses were performed on the three profiles to model conditions prior to the construction of the seepage barrier. The hydraulic conductivity values for the random fill were varied in successive runs of the models for each of the three profiles until the resulting piezometric heads matched the heads measured in the piezometers. The results of these back-analyses are summarized in Table 4-1.

The next step consisted of back-analyses to calculate the effective hydraulic conductivity of the seepage barrier. With the hydraulic conductivity values of the alluvium, bedrock, and random fill held constant, the effects of the construction of the seepage barrier were modeled. The seepage barrier was added to the model and the hydraulic conductivity of the barrier was varied in successive runs for each profile until the resulting piezometric heads matched the heads measured in the piezometers after the seepage barrier was constructed and the reservoir refilled. The seepage barrier hydraulic conductivities calculated from these back-analyses are summarized in Table 4-1.

Key values derived from the results of the seepage analyses are presented in Table 4-2. It can be seen that the maximum exit gradients, at the downstream toe, were reduced by at least half from the original value. High hydraulic gradients were calculated below the barrier, after barrier construction, in locations where the gradients were very low prior to barrier construction. Also, the calculated maximum hydraulic head differentials across the barrier are in excess of 20 feet. With a nominal barrier width of two feet, this head differential results in gradients in excess of 10 across the barrier.

Table 4-1 Hydraulic conductivity results from seepage back-analyses on Upper and Lower Clemson Diversion Dams

Profile	Hydraulic Conductivity (cm/s) Anisotropy Ratio(k_v/k_h)					Seepage Barrier Effective Hydraulic Conductivity
	Basal Sand/ Gravel Alluvium	Silty Sand Alluvium	Silt/Clay/ Sand Alluvium	Bedrock	Random Fill	
Upper Clemson Diversion Dam						
UC-AA	$4.9x10^{-2}$ (0.1)	-	$3.0x10^{-4}$ (0.25)	$3.0x10^{-4}$ (0.25)	$1.5x10^{-3}$ (0.25)	$1.5x10^{-5}$
UC-BB					$1.2x10^{-3}$ (0.25)	$3.0x10^{-5}$
UC-CC					$7.6x10^{-4}$ (0.25)	$6.1x10^{-6}$
Lower Clemson Diversion Dam						
LC-BB	$7.1x10^{-2}$ (0.1)	NA	NA	$3.0x10^{-4}$ (0.25)	$2.5x10^{-3}$ (0.25)	$3.1x10^{-5}$
LC-CC	$1.5x10^{-1}$ (0.1)	$7.1x10^{-2}$ (0.1)	$1.0x10^{-6}$ (0.1)		$1.9x10^{-4}$ (0.25)	$4.7x10^{-5}$
LC-DD	$1.5x10^{-1}$ (0.1)	NA	$1.0x10^{-6}$ (0.1)		$3.1x10^{-3}$ (0.25)	$1.1x10^{-4}$

Two other measures of seepage barrier performance are presented in Table 4-2: the hydraulic conductivity ratio and the head efficiency. Because a design value of hydraulic conductivity was not specified for this seepage barrier, and no hydraulic conductivity tests were performed on the barrier or infill, a value of $1x10^{-8}$ cm/s was assumed based on test results on concrete with no bentonite added (Kaul et al., 1991). The effective hydraulic conductivity values calculated by the back-analyses for these dams were 600 to 11,000 times the estimated hydraulic conductivity values based on these tests on concrete. Head efficiencies of 0.5 to 0.62 were calculated for the six profiles.

Deformation Analyses. Deformation analyses were performed on the same profiles used in the seepage analyses described above. The stages of unloading and loading events modeled consisted of (1) excavation and backfilling of the key trench, (2) construction of the embankment in a total of six layers, (3) filling of the reservoir, and (4) construction of the seepage barrier. In both the reservoir filling and construction of the seepage barrier

stages a single-stage, steady-seepage condition with a full reservoir was modeled in the analyses.

Table 4-2 Key values resulting from seepage analyses on Upper and Lower Clemson Diversion Dams

Profile	Maximum Exit Hydraulic Gradient		Maximum Hydraulic Gradient Below Barrier	Maximum Hydraulic Head Differential Across Barrier (feet)	Hydraulic Conductivity Ratio (Effective over Design)	Head Efficiency
	Before Barrier	After Barrier				
Upper Clemson Diversion Dam						
UC-AA	0.74	0.35	1.7	21	1,500	0.50
UC-BB	0.08	0.04	1.8	21	3,000	0.50
UC-CC	0.83	0.31	1.9	23	610	0.55
Lower Clemson Diversion Dam						
LC-BB	0.77	0.35	1.9	26	3,100	0.62
LC-CC	0.90	0.30	1.9	27	4,100	0.57
LC-DD	0.32	0.15	1.4	19	11,000	0.51

The material properties used in the deformation analyses are presented in Table 4-3. The bedrock was modeled with a linear elastic model specified using values of Young's Modulus and Poisson's Ratio. The alluvium layers and the random fill were modeled using the Duncan and Chang hyperbolic model (Duncan et al. 1980). The Duncan and Chang model is specified using values for Mohr-Coulomb strength parameters (c′ and φ′, Poisson's Ratio, modulus number, modulus exponent, failure ratio, and unloading modulus.

The results of the deformation analyses are summarized in Table 4-4. The calculated maximum deformations are similar for all six profiles. The maximum moments in the seepage barriers are higher for Profiles UC-AA, LC-BB, and LC-CC than for the other profiles. In Profiles UC-AA and LC-CC the large moment is due to the greater thicknesses of the more deformable silt/clay/sand alluvial layers that allow more deformation to occur in the alluvium, thus developing a larger moment at the bedrock interface. In Profile LC-BB the large moment is due to deflection of the embankment fill with a thin layer of alluvium over the bedrock. In all of the profiles the maximum moments were located slightly above the contact between the bedrock and the alluvium.

Table 4-3 Material properties for deformation analyses on Upper and Lower Clemson Diversion Dam

Layer	Behavior Model[1]	c´ (psf)	φ´	Unit Weight (pcf)	Young's Modulus (ksf)	Poisson's Ratio	Modulus Number	Modulus Exponent	Failure Ratio	Unload Modulus Number
Bedrock	LE	50	48	160	80,000	0.15	-	-	-	-
Sand/ Gravel Alluvium	DC	50	38	125	-	0.25	500	0.5	0.8	750
Silty Sand Alluvium	DC	200	34	120	-	0.33	300	0.6	0.7	480
Silt/Clay/ Sand Alluvium	DC	200	30	120	-	0.33	200	0.4	0.75	320
Random Fill	DC	200	34	120	-	0.33	300	0.4	0.75	480

Notes: 1) LE = Linear elastic, DC = Duncan and Chang Hyperbolic (Duncan et al. 1980)

The tensile stresses due to the maximum moment in Profile UC-AA exceed the estimated ultimate tensile strength of the concrete ($f'_t \approx 285$ psi based on an $f'_c \approx 4{,}000$ psi). Calculated tensile stresses in the seepage barrier are shown in Table 4-4. The long-term consequence of this stress condition is likely to be cracking of the barrier near the contact between the bedrock and the alluvial layer.

Table 4-4 Deformation analyses results for seepage barriers in Upper and Lower Clemson Diversion Dams

Profile	Maximum Deformation (in.)	Depth of Maximum Deformation (ft.)	Maximum Moment (ft.·lbs./ft.)	Depth(s) of Maximum Moment (ft.)	Tensile Stress from Moment, Mc/I (psi)	Percentage of Concrete Tensile Strength
Upper Clemson Diversion Dam						
UC-AA	0.2	0	29,489	81	307	108
UC-BB	0.2	0	16,266	83	169	59
UC-CC	0.3	0	17,962	81	187	66
Lower Clemson Diversion Dam						
LC-BB	0.15	0	24,978	81	260	91
LC-CC	0.3	0	23,965	89	250	88
LC-DD	0.2	0	16,882	82	176	62

The deformation analyses did not indicate tensile stresses in excess of the estimated tensile strength in the seepage barrier in the remaining profiles (see Table 4-4). However, variation in the subsurface conditions might result in cracking in adjacent areas. Additionally, stress concentrations near the ends of cracks (such as those calculated to

have developed in Profile UC-AA) may cause cracks to propagate into areas where lower stresses were calculated in the seepage barrier.

Conclusions. The analyses presented above provide insight into the performance of Upper and Lower Clemson Diversion Dams. As stated in Chapter 3, the performance of the Upper and Lower dams and seepage barriers has remained essentially constant since completion of the seepage barriers in 1982 and 1984. However, the seepage analyses indicate that the effectiveness of the barriers in lowering piezometric heads downstream of the barriers is considerably less than might have been anticipated without benefit of back analyses. The effective hydraulic conductivities were calculated to be 600 to 11,000 times the estimated hydraulic conductivity of intact concrete.

There are two likely scenarios that may account for these high values of effective hydraulic conductivity. The first is that cracks have formed in the barriers in the locations of the highly permeable soils at the base of the alluvium. The deformation analyses described above indicate that this is the location that cracking of the barrier is most likely and, in Sections UC-AA the calculated stress in the barrier is large enough to cause cracking. Due to the high permeability of the surrounding soils, significant flow may occur through such a crack, accounting for the higher effective permeability of the barrier.

Analyses were performed to estimate the apertures of cracks needed to account for the increases in effective hydraulic conductivity calculated in the seepage analyses. This calculation is discussed later in this chapter. Assuming that the crack at Section UC-AA was clear of soil particles and planar in shape, and that the Hagan-Poseuille cubic law applies, the crack would only need to be one-tenth of a millimeter wide to produce the effective hydraulic conductivity calculated in the seepage analysis. Larger cracks with irregular shapes and soil infilling would have a similar affect. The analysis resulted in a seepage velocity through the crack of about 0.1 feet per second.

The second scenario is that there may be localized zones of jointed bedrock located near the bases of the seepage barriers that have effective hydraulic conductivities greater than the average value used in the analysis. Several areas within the bedrock in the

downstream portion of the dam foundations were identified as having locally high hydraulic conductivity. Therefore, it is possible that the increased hydraulic gradients developed near the bases of the barriers (calculated as high as 1.9) are increasing the flow through some of these zones and producing the higher piezometric levels that are observed.

Based on these considerations, it appears that either of these scenarios could account for the reduced effectiveness of the seepage barriers. Both scenarios would account for the lack of change in long-term performance of the dams and seepage barriers. In the first scenario, the hydraulic velocity calculated in a crack in a seepage barrier (0.1 feet per second) would not be expected to be high enough to erode the 4000 psi compressive strength concrete. In the second scenario, moderate flow through joints in competent bedrock would not be expected to enlarge the seepage path appreciably and, therefore, the performance of the dam would not be expected to change over time. This result is consistent with the observed long-term behavior of the dam.

Wister Dam

Seepage and deformation analyses were also performed on Wister Dam. The seepage analyses were performed to assess the effectiveness of the barrier in reducing the seepage flow beneath the dam, and to provide data on piezometric heads for use in calculating seepage forces. The deformation analyses were performed to estimate the post-construction deformation of the seepage barrier in order to assess the potential for cracking of the barrier. A description of the materials comprising the dam and foundation is presented in Chapter 3.

Seepage Analyses. The dam and foundation are made up of five components: shale bedrock, alluvium, embankment clay fill, embankment random fill (upstream and downstream berms), and finger drain material. The alluvium was assumed to consist of two units, the upper clayey layer and the basal sand and gravel layer. Although the finger

drains are spaced on 15-foot centers along the length of the dam, they were modeled as a continuous unit.

One profile was selected for this analysis. The profile is located at Station 18+00 near the center of the dam and was selected based on the presence of multiple piezometers and clearly defined clayey and sand/gravel alluvial layers. The seepage analyses were performed with a reservoir level of 475 feet during construction of the barrier and 495 feet before and after construction of the barrier. The tailwater was maintained at elevation 455 feet during all stages. The cross section is shown in Figure 4-4.

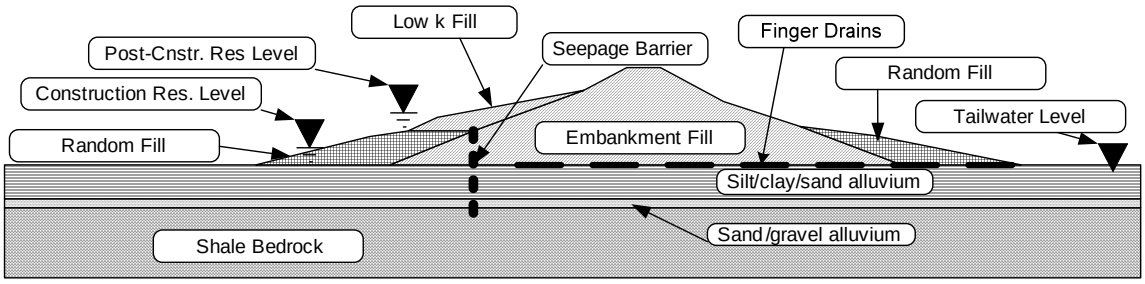

Figure 4-4 Wister dam analysis profile and location (after USACE 1988b, with permission from USACE)

During the initial investigation for the dam construction, pressure leakage tests were performed in the bedrock in 55 bore holes located within the dam footprint (USACE 1959). The tests indicated very little to no leakage in all but two of the bore holes. In the remaining two borings, leakage rates ranging from 9 to 29 gallons per minute were recorded under a pressure of 50 psi. In addition, the bedrock grouting performed in 1949 after the near failure of the dam (see Chapter 3) identified several locations in the bedrock where significant amounts of grout were taken. These facts indicate that the hydraulic conductivity of the bedrock can be expected to vary considerably depending on the presence of joints and the existence and continuity of joint infilling. To account for the uncertainty, several analyses were performed to assess the effects of varying the hydraulic conductivity of the bedrock from $1x10^{-4}$ to $1x10^{-6}$ cm/sec.

The hydraulic conductivity values used in the analyses for the remaining soil units were estimated based on soil descriptions and the results of laboratory gradation tests (USACE

1959). The hydraulic conductivity values used in the analysis of the pre-seepage barrier conditions are listed in Table 4-5. Using these values, an initial back analysis was performed to adjust the hydraulic conductivity of the sand/gravel alluvium so that the results of the analysis matched the observed piezometric levels prior to construction of the seepage barrier. It should be noted that because the hydraulic conductivity of the sand/gravel alluvium was much greater than that of the bedrock, the variation of the bedrock hydraulic conductivity without the seepage barrier had no significant effect on the results of the pre-seepage barrier analyses.

Table 4-5 Hydraulic conductivity values used in seepage back-analyses on Wister Dam

Unit	Sand/ Gravel Alluvium	Clayey Alluvium	Embankment Clay Fill	Embankment Random Fill	Finger Drains
Hydraulic Conductivity (cm/s)	$1x10^{-2}$	$1x10^{-6}$	$1x10^{-6}$	$1x10^{-2}$	$1.3x10^{-6}$
Anisotropy Ratio(k_v/k_h)	0.1	0.1	0.25	0.25	0.1

Back-analyses where performed to calculate the effective hydraulic conductivity of the seepage barrier using a range of bedrock hydraulic conductivity values while holding the hydraulic conductivity values of the alluvium, and embankment fills constant. The seepage barrier was added to the model and the hydraulic conductivity of the barrier was varied in successive runs until the resulting piezometric heads matched the measured heads. The seepage barrier hydraulic conductivities calculated from these back-analyses are summarized in Table 4-6.

In addition to the effective hydraulic conductivity results for the seepage barriers, other key values derived from the results of the seepage analyses are presented in Table 4-6. The maximum exit gradients before and after the construction of the seepage barrier were less than 0.1 before and after seepage barrier construction. However, high hydraulic gradients varying from 1.6 to 3.7 were calculated below the barrier in locations where the gradients were low prior to barrier construction. Also, the calculated maximum hydraulic

head differentials across the barrier are 17 feet or more. With a nominal barrier width of two feet, this head differential results in gradients in excess of eight across the barrier.

Table 4-6 Key values resulting from seepage analyses on Wister Dam

Bedrock Hydraulic Conductivity (cm/s)	Effective Seepage Barrier Hydraulic Conductivity (cm/s)	Seepage Barrier Hydraulic Conductivity Ratio (Effective over Design)	Maximum Hydraulic Gradient Below Barrier	Maximum Hydraulic Head Differential Across Barrier (feet)	Head Efficiency
$1x10^{-4}$	$3x10^{-6}$	300	1.6	18.5	0.46
$1x10^{-5}$	$2x10^{-5}$	2,000	2.9	17.0	0.42
$1x10^{-6}$	$2x10^{-5}$	2,000	3.7	18.0	0.45

Two other values are presented in Table 4-6 that are measures of the seepage barrier performance: the hydraulic conductivity ratio and the head efficiency. Because a value of hydraulic conductivity was not specified for this seepage barrier and no hydraulic conductivity tests were performed on the barrier or infill, a value of $1x10^{-8}$ cm/s was assumed based on test results on plastic concrete presented by Kaul et al. (1991). The effective hydraulic conductivity values calculated by the back-analyses for this dam were 300 to 2,000 times the estimated hydraulic conductivity based on Kaul et al.'s tests.

Head efficiencies of 0.42 to 0.46 were calculated from the results of the analyses. The small range in head efficiency values is expected because the analyses were all back calculated to fit the same data from piezometers located in the central and downstream portions of the dam. The head values for calculating the differential head across the barrier and the head efficiency are taken directly upstream and downstream of the barrier where no piezometers were located. Therefore, the small variation in the calculated head efficiency values is the result of different seepage pathways in the various model results that result in head losses occurring in differently along the seepage paths. This results in slightly different differential head values across the barrier and leads to the variation in head efficiency.

Deformation Analyses. Because the value of hydraulic conductivity used for the bedrock in the above analyses did not significantly affect the resulting piezometric pressure regime before and after seepage barrier construction, deformation analyses were performed using the piezometric pressures calculated for the model with a bedrock hydraulic conductivity value of $1x10^{-6}$ cm/sec. The stages modeled were: 1) construction of the embankment, 2) initial filling of the reservoir, 3) lowering of the reservoir, 4) excavation of the work platform for seepage barrier construction, 5) construction of the seepage barrier, 6) construction of embankment fill above the seepage barrier, and 7) refilling of the reservoir. In stages 1, 2, 3, 5, and 7 the piezometric pressure regime in the dam was estimated from the steady seepage analyses.

The material properties used in the deformation analyses are presented in Table 4-7. The bedrock was modeled as a linear elastic material using values of Young's Modulus and Poisson's Ratio. The alluvium layers and the random fill were modeled using the Duncan and Chang Hyperbolic model (Duncan et al. 1980). The Duncan and Chang model is specified using values of Poisson's Ratio, modulus number, modulus exponent, failure ratio, and unloading modulus.

Table 4-7 Material properties for deformation analyses on Wister Dam

Layer	Behavior Model[1]	c´ (psf)	φ´	Unit Weight (pcf)	Young's Modulus (ksf)	Poisson's Ratio	Modulus Number	Modulus Exponent	Failure Ratio	Unloading Modulus
Shale Bedrock	LE			160	140,000	0.25	-	-	-	-
Sand/Gravel Alluvium	DC			125	-	0.26	1000	0.5	0.7	1600
Clayey Alluvium	DC			120	-	0.37	200	0.5	0.5	400
Embankment Clay Fill	DC			120		0.35	200	0.5	0.5	400
Embankment Random Fill	DC			120	-	0.35	200	0.3	0.7	320

Notes: 1) LE = Linear elastic, DC = Duncan and Chang Hyperbolic (Duncan et al. 1980)

The results of the deformation analyses are presented in Table 4-8. The maximum moment of 16,000 foot pounds per linear foot of barrier occurs at a depth of about 52 feet below the top of the barrier, near the top of the bedrock. Based on the average result of the compressive strength tests performed on the barrier infill during construction of about

1000 psi (144,000 psf), the tensile strength of the barrier was estimated to be about 142 psi (20,000 psf). Using this tensile strength and neglecting the axial forces in the barrier, the moment required to result in rupture of the barrier is expected to be on the order of 14,000 foot pounds per linear foot of barrier. Thus, based on this deformation analysis, cracking of the barrier would be expected to occur due to the stresses induced by the differential water loads.

Table 4-8 Deformation analyses results for seepage barrier in Wister Dam

Maximum Deformation (in.)	Depth of Maximum Deformation (ft.)	Maximum Moment (ft.·lbs./ft.)	Depth(s) of Maximum Moment (ft.)	Tensile Stress Due to Moment, Mc/I (psi)	Percentage of Concrete Tensile Strength
0.4	0	16,000	52	167	117

Conclusions. The seepage analyses using a range of hydraulic conductivity values for the bedrock provided some insight into the factors that affect the measures of seepage barrier effectiveness (i.e. effective hydraulic conductivity and head efficiency). When a high value of hydraulic conductivity was used for the bedrock, the analysis resulted in a lower effective seepage barrier hydraulic conductivity than the analyses using lower bedrock hydraulic conductivity values. This effect is due to a larger amount of the flow occurring through the high hydraulic conductivity bedrock.

The use of different hydraulic conductivities in the bedrock also affected the resulting hydraulic gradients below the barrier. Greater seepage resistance through the bedrock due to lower hydraulic conductivity results in higher gradients in the bedrock. Thus, in the case where the bedrock seepage resistance is decreasing due to soil infill being eroded from bedrock joints, the hydraulic gradient and erosion potential will decrease as the erosion progresses. This relationship has an effect on how much erosion will take place before a state of equilibrium is reached between the eroded material and the seepage velocity.

The head efficiency of the seepage barrier does not appear to be significantly affected by the hydraulic conductivity of the barrier. All of the analyses were back calculated to match the water pressure regime indicated by the piezometers.

The deformation analysis indicates that the calculated deformation of the barrier is likely to cause the barrier to crack. It has been shown in previous analyses that even a small crack has the potential to increase the effective hydraulic conductivity of the seepage barrier significantly. Therefore, it is possible that the increase in effective hydraulic conductivity is due to cracks developing in the barrier due to deformation. However, it is also possible that higher than anticipated seepage through joints in the bedrock is the cause of the higher effective hydraulic conductivity. Down-hole water pressure tests and records of grout takes indicate that, while the bedrock appears to be generally tight, there are zones where there appear to be open joints. The actual cause of the increase in effective hydraulic conductivity of the barrier is likely a combination of the cracking and the joints in the bedrock.

Fontenelle Dam

The seepage analysis of Fontenelle Dam is trivial due to the several orders of magnitude difference that exists between the hydraulic conductivity of the open fractured bedrock and the hydraulic conductivity of the seepage barrier, the Zone 1 fill, and the less fractured (tight) bedrock. The consequence of this large difference is that changes of up to two orders of magnitude in the hydraulic conductivity of the fractured bedrock or seepage barrier have little effect on the hydraulic heads and gradients calculated by the analyses. In any case, the observed seepage conditions in the dam show nearly 100 percent efficiency of the barrier. This efficiency is confirmed by actual piezometer readings (see details in Chapter 3).

It was desired to perform analyses to assess wall deformation under the high differential water pressure loading so that a comparison could be made between the calculated deformations and the deformations detected by inclinometers installed within the barrier.

In order to perform the deformation analyses, it was necessary to develop pore water pressure values at each node of the finite element grid to use in calculating forces due to differential water pressures (seepage and buoyant forces). These water pressures were calculated by performing a seepage analysis with assumed hydraulic parameters for the various units that resulted in a seepage regime similar to that indicated by the piezometers. The deformation analyses were then performed to estimate the post-construction deformation of the seepage barrier, to assess the potential for cracking of the barrier, and to assess where cracking is likely to occur.

Deformation Analyses. The analyses were performed on a cross section near the center of the dam where the barrier is near its full depth. The cross section used in the analysis is shown in Figure 4-5. A full description of the materials comprising the dam and foundation is presented in Chapter 3.

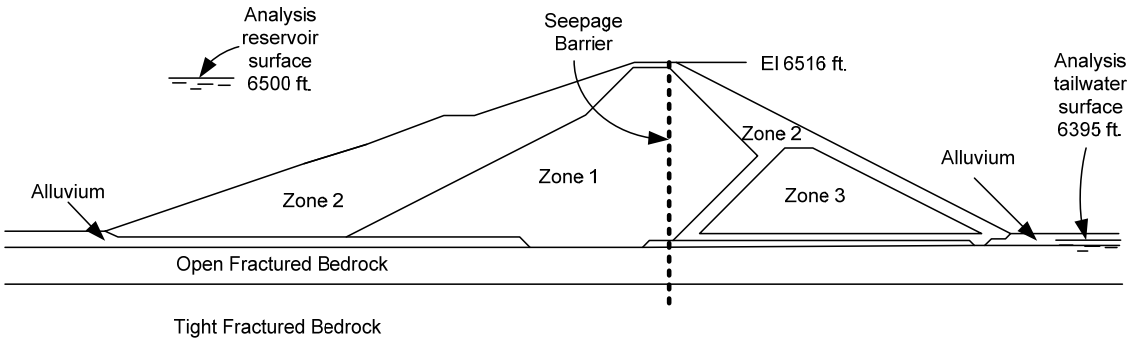

Figure 4-5 Cross section of Fontenelle Dam used in the deformation analysis (modified from USBOR 2002, with permission from USBOR)

The loading events modeled consisted of (1) constructing the embankment in seven layers, (2) filling the reservoir, and (3) constructing the seepage barrier. In both the reservoir filling and construction of the seepage barrier stages a steady-state seepage condition with a full reservoir was assumed.

The material properties used in the deformation analyses are presented in Table 4-9. The highly fractured and less fractured bedrock layers were modeled with a linear elastic

model specified using values of Young's Modulus and Poisson's Ratio. The three zones of the embankment and the alluvium were modeled using the Duncan and Chang hyperbolic model (Duncan et al. 1980). The Duncan and Chang model is specified using values of Mohr-Coulomb strength parameters c′ and φ′, Poisson's Ratio, modulus number, modulus exponent, failure ratio, and unloading modulus.

Table 4-9 Material properties for deformation analyses on Fontenelle Dam

Layer	Behavior Model[1]	c′ (psf)	φ′	Unit Weight (pcf)	Young's Modulus (ksf)	Poisson's Ratio	Modulus Number	Modulus Exponent	Failure Ratio	Unloading Modulus Number
Highly Fractured Bedrock	LE	200	45	145	140,000	0.20	-	-	-	-
Less Fractured Bedrock	LE	200	45	145	140,000	0.20	-	-	-	-
Zone 1 - Core	DC	200	30	120	-	0.33	200	0.5	0.65	350
Zone 2 – Shell	DC	100	35	125	-	0.27	450	0.6	0.8	650
Zone 3 – Random Fill	DC	100	35	125	-	0.28	400	0.5	0.7	600

Notes: 1) LE = Linear elastic, DC = Duncan and Chang Hyperbolic (Duncan et al. 1980)

The results of the deformation analyses are shown in Table 4-10. The tensile stresses due to the maximum moments calculated near the interface between the embankment and the foundation resulted in a tensile stress in the seepage barrier that exceeds the estimated ultimate tensile strength of the concrete ($f'_t \approx 285$ psi (41,000 psf) based on an $f'_c \approx 4{,}000$ psi). The long-term consequence of this stress condition is likely to be cracking of the barrier near embankment/foundation interface.

Table 4-10 Deformation analyses results for seepage barrier in Fontenelle Dam

Maximum Deformation (in.)	Depth of Maximum Deformation (ft.)	Maximum Moment (ft.·lbs./ft.)	Depth of Maximum Moment (ft.)	Induced Tensile Stress, Mc/I (psi)	Percentage of Concrete Tensile Strength
1.1	64	51,362	130	535	188

Conclusions. The deformation analyses presented above result in a bow-shaped deformation pattern similar to that observed in five of the six inclinometers in the dam.

The calculated magnitude of deformation is about twice that measured in the inclinometers. This discrepancy may be due to one or a combination of the following factors:

- The parameters used in the model result in the stiffness of the Zone 1 material being less than the actual stiffness, and
- The model assuming a steady state seepage condition which will result in higher water pressures upstream of the barrier and lower water pressures downstream of the barrier in the Zone 1 material.

Nevertheless, obtaining results that show the same deformation pattern and similar magnitude of deformation suggests that the analyses provide a reasonable estimate of the effects of the differential water pressures on the barrier deformation.

The analyses indicate that moments developed by the deformation of the seepage barrier were great enough to result in tensile stresses that are sufficient to cause cracking of the concrete barrier. The locations of these stresses are in the area of the interface between the Zone 1 material and the foundation. The piezometer readings indicate that seepage is occurring in this area either through the barrier or in the bedrock below the barrier. Thus, the modeled cracking of the barrier in this area represents a plausible explanation for the observed behavior in this area.

The most compelling evidence of barrier leakage occurs within the Zone 1 material (see assessment of performance in Chapter 3). While the analyses do not indicate that moments in this area are large enough to result in barrier cracking, the barrier deformations are largest in this area. Based on these results, in may be hypothesized that the barrier leaks in this area are due to one or a combination of the following:

- Cracking of the barrier due to stress concentrations caused by localized variation in the stiffness of the Zone 1 material,
- Gaps developing between barrier panels due to differential movement of the individual wall panels, and
- Construction defects.

Thus, it is possible that the observed barrier leakage is a result of the modeled deflections.

Navajo Dam

Two factors make performing a meaningful seepage analysis on Navajo Dam difficult. First, the seepage barrier does not extend across the entire length of dam and the barriers length is only slightly more than its height. Therefore, seepage around the end of the barrier has a significant effect on the seepage regime. Second, the hydraulic conductivity parameters of the most critical part of the model, the bedrock, are controlled by jointing and open bedding planes and, consequently, can vary a great deal over short distances. For these reasons, neither the efficiency of the barrier nor the effective hydraulic conductivity of the barrier infill can be assessed with the level of precision needed to make the analysis relevant.

It was desired to perform analyses to assess wall deformation under the high differential water pressure loading in the bedrock, and to evaluate cracking potential under this loading. To perform the deformation analyses, it was necessary to develop pore water pressure values at each node of the finite element grid in order to calculate forces due to differential water pressures (seepage and buoyant forces). These water pressures were calculated by performing a seepage analysis in which the hydraulic parameters for the various units were varied using repeated trials until water pressure regimes were obtained that were similar to those shown by the piezometers before and after seepage barrier construction. The deformation analyses were then performed to estimate the post-construction deformation of the seepage barrier, assess the potential for cracking of the barrier, and assess where the cracking is likely to occur.

Deformation Analyses. The analyses were performed on a cross section near the right end of the dam where the barrier extended full depth. The cross section used in the analysis is shown on Figure 4-6. A full description of the materials comprising the dam and foundation is presented in Chapter 3.

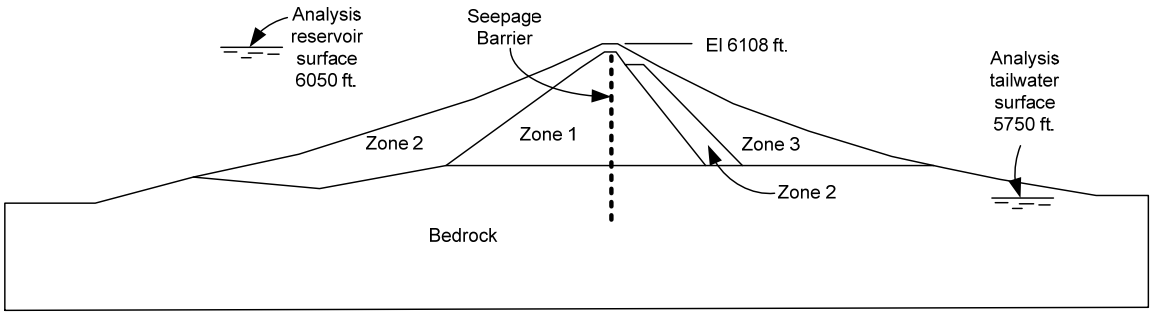

Figure 4-6 Cross section of Navajo Dam used in the deformation analyses.

The sequence of events modeled was (1) constructing the embankment in six layers, (2) filling the reservoir, and (3) constructing the seepage barrier. In both the reservoir filling and construction of the seepage barrier stages steady-state seepage conditions with a full reservoir were used to model the seepage regime.

The material properties used in the deformation analyses are presented in Table 4-11. The bedrock was modeled with a linear elastic model specified using values of Young's Modulus and Poisson's Ratio. Because the bedrock varies from sandstone to shale, the stiffness of the bedrock is likely to vary. Therefore, the model was analyzed three times using values for Young's Modulus ranging from 140,000 ksf (representative of the sandstone) to 14,000 ksf (representative of the shale).

The three zones of the embankment were modeled using the Duncan and Chang hyperbolic model (Duncan et al. 1980). The Duncan and Chang model is specified using values of Mohr-Coulomb strength parameters c′ and φ′, Poisson's Ratio, modulus number, modulus exponent, failure ratio, and unloading modulus. Considering descriptions of the soil type, the method of placement, and the compaction effort for the three zones of the embankment, estimates of the Duncan and Chang parameters for the embankment soils were selected based on typical values for similar soils and the correlations presented in Duncan and Wong (1999). These initial parameter estimates are presented in Table 4-11.

Table 4-11 Material properties for deformation analyses on Navajo Dam

Layer	Behavior Model[1]	φ	c' (psf)	Unit Weight (pcf)	Young's Modulus (ksf)	Poisson's Ratio	Modulus Number	Modulus Exponent	Failure Ratio	Unloading Modulus Number
Bedrock	LE	50	200	145	14,000 70,000 140,000	0.20	-	-	-	-
Initial Estimates										
Zone 1 - Core	DC	30	200	120	-	0.33	200	0.5	0.65	350
Zone 2 – Shell	DC	38	100	125	-	0.27	450	0.6	0.8	650
Zone 3 – Random Fill	DC	35	100	125	-	0.28	400	0.5	0.7	600
Adjusted Parameters to Match Observed Deflections										
Zone 1 - Core	DC	25	100	120	-	0.35	30	0.5	0.5	50
Zone 2 – Shell	DC	35	0	125	-	0.27	400	0.6	0.7	600
Zone 3 – Random Fill	DC	35	0	125	-	0.28	400	0.5	0.7	600

Notes: 1) LE = Linear elastic, DC = Duncan and Chang Hyperbolic (Duncan et al. 1980)

The results of the deformation analyses using the initial parameter estimates are presented in Table 4-12. The tensile stresses that result from the maximum bending moments for all three bedrock stiffnesses resulted in total tensile stresses in the seepage barrier below the estimated ultimate tensile strength of the concrete ($f'_t \approx 285$ psi (41,000 psf) based on $f'_c \approx 4{,}000$ psi). However, the model with the stiffest bedrock resulted in tensile stresses that are essentially the same as the estimated tensile strength of the barrier concrete. The resulting deflected shape of the barrier is similar to that measured with the inclinometers in the seepage barrier; displacements starting at the bedrock interface and increasing with increasing elevation, resulting in a maximum deflection at the top of the barrier. However, the magnitudes of the displacements were much less than those observed in the inclinometers (maximum displacement of up to 8 inches).

Because the results of the analyses with the initial parameters resulted in displacements much lower than those observed in the dam, the parameters of the embankment soils were modified in repeated trials until the resulting deformations matched the observed displacements. The resulting parameters are presented in the lower portion of Table 4-11 and the results of these analyses are presented in the lower portion of Table 4-12. The

parameters that resulted in the displacements similar to those measured in the inclinometers represent the low end of the range of the parameters presented in Duncan and Wong (1999) for similar soils.

Table 4-12 Deformation analyses results for seepage barrier in Navajo Dam

Modulus in Bedrock (ksf)	Maximum Deformation (in.)	Depth of Maximum Deformation (ft.)	Maximum Moment (ft.·lbs./ft.)	Depth(s) of Maximum Moment (ft.)	Induced Tensile Stress from Moment Mc/I (psf)	Percentage of Concrete Tensile Strength
Analyses with Initial Parameter Estimates						
14,000	1.6	0	24,800	273	84	29
70,000	1.4	0	23,800	273	81	28
140,000	1.2	0	83,200	273	283	99
Analyses with Parameters to Match Observed Displacements						
14,000	7.7	0	492,000	273	1,670	585
70,000	7.0	0	524,000	273	1,780	624
140,000	6.0	0	599,000	273	2,040	715

Conclusions. The analyses described above illustrate the effect soil parameters have on the behavior of the seepage barrier. When the initial estimates of the embankment soil parameters were used in the model, the moments induced in the seepage barrier were well below to slightly below the estimated moment needed to crack the barrier. Additional analyses performed using the low end of the range of parameters (most deformable) resulted in deformations that were similar to those measured by the inclinometers. Hence, while the parameters needed to match the observed behavior where much lower than the initial estimates, they were still within the range of published values for similar soil types.

Several factors may explain the high deformation potential of the embankment soils. First, the final construction report for the dam (USBOR 1963) states that the embankment construction occurred year-round and was only halted a few times during heavy rain and snow events. This year-round construction may have resulted in compaction water contents significantly above the optimum that would tend to increase the deformability of the dam. A second reason for higher deformability may be disturbance of the soils during

construction of the seepage barrier. The barrier in Navajo Dam extends much deeper than others and, as a result, the zone of deformation due to relaxation of the embankment fill soil into the slurry-supported excavation may be wider than in other dams. When the reservoir loads are applied to the barrier, the disturbance that occurred due to the relaxation may result in higher than expected deformation. The third reason may be that the mineralogy of the core material may be such that the soil is more deformable than the average compacted clay core. It may also be that a combination of these factors may explain the high deformability of the embankment.

The analyses using the initially estimated parameters resulted in stresses in the seepage barrier that were either very close to the estimated tensile strength of the barrier concrete (when a Young's Modulus value of 140,000 ksf was used to model the bedrock) or below the barrier concrete tensile strength (when lower values of Young's Modulus were used). When the parameters were adjusted to match the maximum observed deformations in the seepage barrier, the resulting tensile stresses were much greater than the estimated tensile strength of the barrier concrete. Thus, the analyses indicate that there is a high likelihood for cracking in the barrier at the interface between the bedrock and the embankment.

The locations of cracks in core holes drilled in the seepage barrier after completion of the seepage barrier are shown on Figure 4-7. It can be noted that the one open crack detected (bottom of Core 14), the largest concentration of cracks (Core 04), and one of the four low velocity zones detected (Core 06) were all located near the contact between the embankment and the bedrock. Minor cracks were detected at this contact in 6 of the 11 cores that crossed the contact

Numerous additional cracks were also detected in the seepage barrier in locations away from the embankment/foundation interface. The cracks in these locations appear to be randomly distributed. However, a large portion of the cracks located where the barrier is embedded in the bedrock appear to be aligned on horizontal planes. Eight dashed lines drawn through the bedrock portion of the seepage barrier on Figure 4-7 intercept or are very close to a majority of the cracks in the bedrock. This alignment may be caused by

differential deflection of the barrier due to the varying stiffness of the interbedded sandstone and shale layers. The high differential water pressure measured across the barrier tends to push the barrier into the bedrock on the downstream side of the barrier. The shale on the downstream side of the barrier, being less stiff, deforms more than the sandstone, resulting in stress concentrations near the contacts between the two rock types.

.

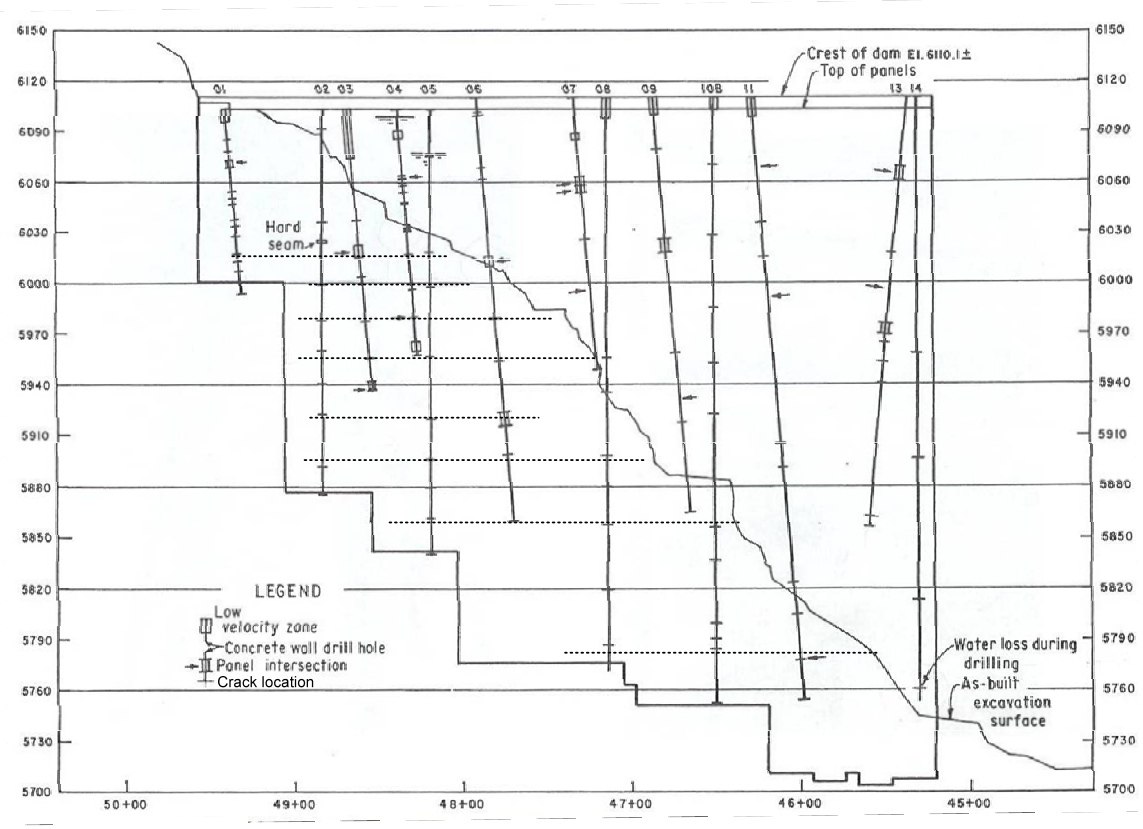

Figure 4-7 Detected crack locations in seepage barrier core holes (modified from Davidson 1990, with permission from USSD)

Regardless of the cause of the observed cracking, the consequences of the seepage barrier cracking are small. Piezometer data indicate that a large difference in water pressure exists across the barrier. This indicates that the barrier has an effective hydraulic conductivity much lower than the surrounding bedrock. The measured piezometric levels in the bedrock indicate that the seepage barrier has an efficiency of up to 55 percent, even with the effects of seepage around the end of the barrier.

Virginia Smith Dam

Seepage analyses were performed for Virginia Smith Dam to assess the effectiveness of the barrier and the effective permeability of the seepage barrier backfill. The dam, the foundation, and the seepage barrier are described in Chapter 3.

Seepage Analyses. Two cross sections through Virginia Smith Dam were analyzed to assess the behavior of the fully-penetrating and partially-penetrating reaches of the seepage barrier. Both cross sections are shown in Figure 4-8. At the first cross section, near Station 29+00, the seepage barrier extends down to bedrock. The soil-bentonite barrier in this cross section is five feet thick. The lower portion of the alluvium in this area consists of coarse sand and gravel with high permeability. At the second cross section, near Station 50+00, the three-foot thick, soil-bentonite barrier extends to a depth of 45 feet and the alluvium extends to a depth of over 100 feet. The alluvium near Station 50+00 consists of interbedded fine sand and silty sand and has a much lower permeability than the deeper alluvium at Station 29+00. Both cross sections are shown in Figure 4-8.

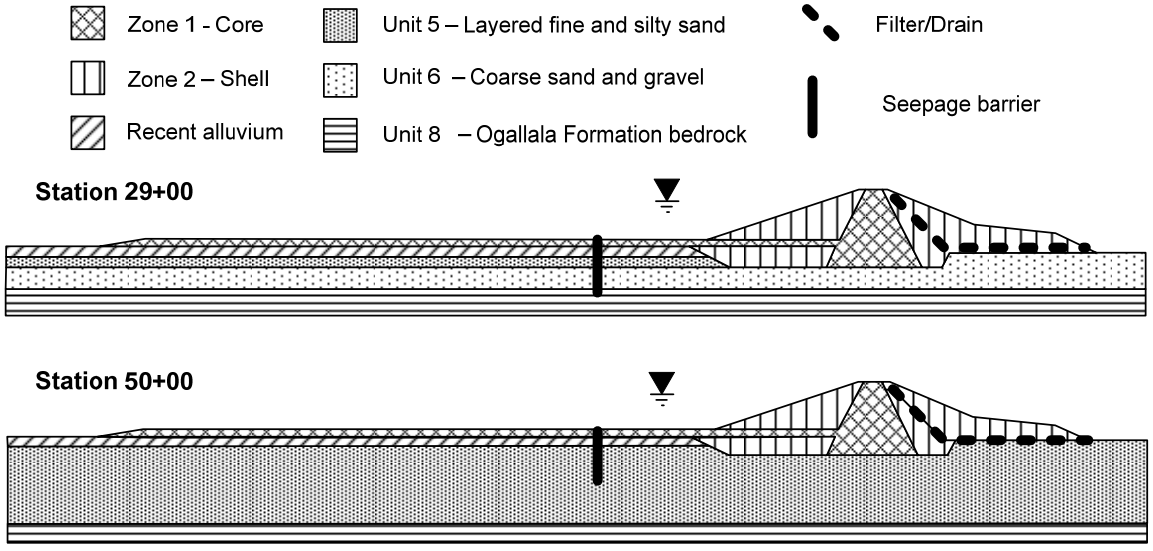

Figure 4-8 Two analysis cross sections for Virginia Smith Dam

During design of the dam, field pumping tests were performed in the alluvium to measure the hydraulic conductivity of the various alluvium and bedrock layers. Laboratory testing

was performed to assess the hydraulic conductivity of the various zones of the dam embankment. Based on the results of these tests, the Bureau of Reclamation assigned hydraulic conductivity and anisotropy ratio (ratio of vertical to horizontal hydraulic conductivity) values to the various soils in the embankment and foundation (USBOR 1983). These values are listed on Table 4-13. The Bureau of Reclamation values were used in the initial seepage analyses performed for this study.

Table 4-13 Hydraulic conductivity values used in first round of seepage analyses for Virginia Smith Dam

Soil Type	Horizontal Hydraulic Conductivity (cm/sec)	Ratio of Vertical to Horizontal Hydraulic Conductivity (k_v/k_h)
Embankment Zone 1 – Core	$1.7x10^{-6}$	0.25
Embankment Zone 2 – Shell	$1.1x10^{-3}$	0.25
Embankment Filter/Drain	$1.3x10^{-1}$	1
Seepage Barrier Infill	$1.7x10^{-6}$	1
Units 2 and 3 - Recent Alluvium (near surface)	$2.8x10^{-1}$	0.04
Unit 5 - Interbedded Fine Sand and Silty Sand	$1.1x10^{-2}$	0.02
Unit 6 - Coarse Sand and Gravel	$1.3x10^{-1}$	0.1
Unit 8 – Ogallala Bedrock	$3.3x10^{-3}$	0.04

The results of the analyses using the hydraulic conductivity values in Table 4-13 are summarized in Table 4-14. In addition to the initial analyses, analyses were performed on both models to assess the effects of increasing the values of hydraulic conductivity of the seepage barrier backfill and the foundation material at the base of the barrier. For the model at Station 29+00 (fully penetrating), one analysis was performed with the barrier backfill hydraulic conductivity increased by a factor of 10 and another analysis was performed with the bedrock hydraulic conductivity increased by a factor of 10. For the model at Station 50+00 (partially penetrating), an analysis was performed with the barrier backfill hydraulic conductivity reduced by a factor of 10 and another analysis performed with the ratio of the vertical to horizontal hydraulic conductivities increased by a factor of 10 (resulting in a 10-fold increase in the vertical hydraulic conductivity). The results of these analyses are shown in Table 4-14.

Table 4-14 Results of seepage analyses for Virginia Smith Dam

Model	Differential Hydraulic Head Across the Seepage Barrier (feet)	Maximum Gradient Around Toe of the Seepage Barrier
Station 29+00 (Fully Penetrating)		
Using hydraulic conductivity parameters presented in Table 4-13 (initial model)	40	5.2
Using $1.7x10^{-5}$ cm/s for barrier backfill hydraulic conductivity	38	4.9
Using $3.3x10^{-2}$ cm/s for Unit 8 hydraulic conductivity	16	1.2
Station 50+00 (Partially Penetrating)		
Using hydraulic conductivity parameters presented in Table 4-13 (initial model)	19	0.4
Using $1.7x10^{-5}$ cm/s for barrier backfill hydraulic conductivity	15	0.4
Using 0.2 for Unit 5 k_v/k_h ratio	8	0.2

Conclusions. The analysis performed at Station 29+00 using the Bureau of Reclamation parameters resulted in differential water pressure across the seepage barrier similar to the upper end of values observed by piezometers soon after construction in the fully penetrating portion of the seepage barrier (three sets of piezometers indicated differential hydraulic heads across the barrier of 10 to 40 feet in this area, see Chapter 3). This indicates that, for portions of this reach, the model and parameters model the actual conditions accurately. The additional two analyses were performed to assess variations from the initial model that might account for the lower values observed in other areas (i.e. differential head of 10 feet). The results of these analyses indicate that a 10-fold increase in the hydraulic conductivity of the seepage barrier backfill has a small effect on the analysis results, while changing the hydraulic conductivity of the bedrock at the base of the wall has a much larger effect on the results. These results suggest that the reason for lower differential head values in some locations is more likely to be the result of variation in the bedrock than variation of the seepage barrier backfill. Such bedrock variations could be due to vertical joints or sandy layers. One additional factor that was not modeled is the three dimensional effect where head differentials may be decreased due to flow around the end of the fully-penetrating reach of the barrier.

The analysis performed using the Bureau of Reclamation parameters at Station 50+00 resulted in differential water pressure across the partially penetrating portion of the seepage barrier that were significantly higher than the observed values (one set of piezometers indicated very small differential hydraulic head across the barrier in this area, see Chapter 3). The additional two analyses were performed to investigate the potential causes for this discrepancy. The results of these analyses indicate that changes in seepage barrier backfill hydraulic conductivity have a small effect on the results while changes in the vertical hydraulic conductivity of the material surrounding the lower portion of the barrier had a larger effect. However, both of these analyses resulted in higher differential hydraulic heads than indicated by the piezometers. These results indicate that the horizontal and vertical hydraulic conductivity of the Unit 5 material may be underestimated in the model, at least at the locations of the piezometers.

The greatest difference between the results of the partially and fully-penetrating seepage barriers is in the gradient below the wall. Much higher gradients were calculated in the bedrock at the base of the fully-penetrating barrier than at the base of the partially penetrating barrier, even when the differential hydraulic head values are similar. The consequence of this result is that the potential for internal erosion is much greater at the base of the fully penetrating barrier, assuming equal erodibility of the material beneath the barrier. These high gradients, combined with a pathway for removing infill from bedrock joints or erodible bedrock, have the potential to decrease the efficiency of the seepage barrier over time.

Manasquan Dam

Seepage analyses were performed for Manasquan Dam to assess the effectiveness of the barrier and the effective permeability of the seepage barrier backfill. The dam, the foundation, and the seepage barrier are described in Chapter 3.

Seepage Analyses. Two cross sections through Manasquan Dam were analyzed to assess the behavior of the seepage barrier. The two cross sections are presented in Figure 4-9. At the first cross section, near Station 10+00, the seepage barrier is keyed into the clay of the Upper Mansquan Formation. The barrier in this cross section is 3 feet wide. At the second cross section, near Station 16+00, the upper Manasquan Formation had been previously mined away and had to be replaced with a low-permeability clay blanket that ties into the Manasquan Formation beyond the limits of the mining. The barrier at Station 16+00 is five feet wide and ties into a thickened portion of the seepage blanket.

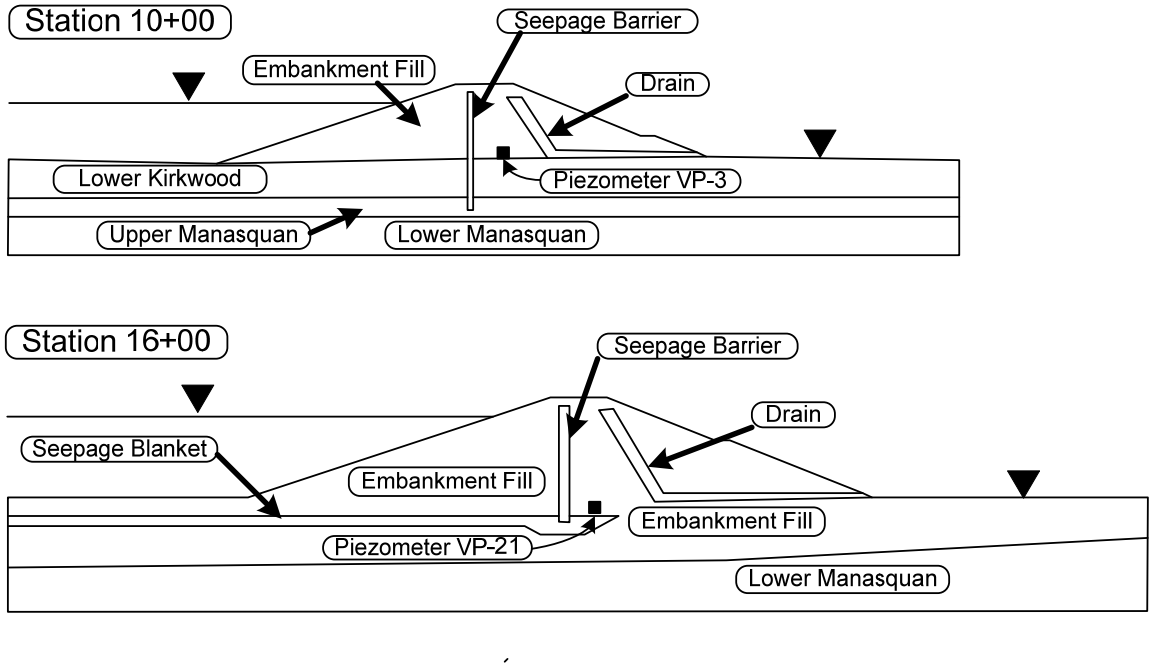

Figure 4-9 Manasquan Dam analysis cross sections at Stations 10+00 and 16+00

During design of the dam, in-situ borehole falling-head and rising-head permeability tests were performed in the Upper and Lower Kirkwood, Upper and Lower Manasquan, and Vincentown Formations (Woodward-Clyde Consultants 1984). Based on the average of the results of several tests in each formation, values of horizontal hydraulic conductivity were selected for use in the analyses. Anisotropy ratios, the ratio of vertical to horizontal hydraulic conductivity, were estimated by Woodward-Clyde Consultants (1984) based on the variation of soils observed in exploratory borings. The resulting values are shown in Table 4-15. Laboratory testing was performed to assess the hydraulic conductivity of the

embankment fill. These tests resulted in hydraulic conductivity values of about 1 x 10^{-3} cm/sec (Woodward-Clyde Consultants 1984). Based on descriptions of the chimney and blanket drain material, a hydraulic conductivity of 1.0 cm/sec was estimated.

Table 4-15 Hydraulic conductivity values used in first round of analyses for Manasquan Dam

Soil Type	Horizontal Hydraulic Conductivity (cm/sec)	Ratio of Vertical to Horizontal Hydraulic Conductivity (k_v/k_h)
Lower Kirkwood Formation	$5.0x10^{-4}$	0.1
Upper Manasquan Formation	$2.0x10^{-6}$	0.25
Lower Manasquan Formation	$1.0x10^{-4}$	0.1
Embankment Fill	$1x10^{-3}$	0.25
Chimney and Blanket Drains	1.0	1.0

Using the hydraulic conductivities and anisotropy ratios (k_v/k_h) presented in Table 4-15, seepage analyses were performed on the two profiles presented in Figure 4-9 using a range of hydraulic conductivity values for the seepage barrier. For each of the analyses the head at the location of a piezometer located just downstream of the seepage barrier (Piezometer VP-3 at Station 10+00 and VP-21 at Station 16+00) was noted for comparison with the measured values. The locations of these piezometers are shown on Figure 4-9. The results of these analyses are summarized in Table 4-16.

The results of the analyses performed on both cross sections indicate that a change in the hydraulic conductivity of the seepage barrier from $1x10^{-7}$ to $1x10^{-6}$ cm/sec results in very small changes in the calculated heads downstream of the seepage barrier. As the value of seepage barrier hydraulic conductivity increases, larger values of head were calculated. The analyses performed on the Station 10+00 cross section resulted in head values close to the measured head value for hydraulic conductivities of $1x10^{-7}$ to $1x10^{-6}$ cm/sec.

For the Station 16+00 cross section the values closest to the measured value were for seepage barrier hydraulic conductivity values between $1x10^{-7}$ to $1x10^{-5}$ cm/sec. Because analyses performed using a large range of seepage barrier hydraulic conductivity values produce hydraulic heads that are within the range of precision of piezometer

measurements, it not possible to assess the effective hydraulic conductivity closer than one or two orders of magnitude. The wide range of possible hydraulic conductivities for the seepage barrier backfill is a result of the large difference in hydraulic conductivity between the seepage barrier backfill and the embankment and foundation soils.

Table 4-16 Results of seepage analyses for Manasquan Dam

Cross Section at Station 10+00			
Seepage Barrier Hydraulic Conductivity Used (cm/sec)	Calculated Head at Piezometer VP-3 (ft.)	Measured Head in Piezometer VP-3 (ft.)	Hydraulic Gradient below Base of Seepage Barrier
$1x10^{-7}$	76.2	75	1.9
$1x10^{-6}$	76.6		1.8
$1x10^{-5}$	79.5		1.2
$1x10^{-4}$	84.5		0.6
$1x10^{-3}$	87.9		0.4
Cross Section at Station 16+00			
Seepage Barrier Hydraulic Conductivity Used	Calculated Head at Piezometer VP-21 Location (ft.)	Measured Head in Piezometer VP-21 (ft.)	Hydraulic Gradient below Base of Seepage Barrier
$1x10^{-7}$	61.6	64	3.5
$1x10^{-6}$	62.0		3.5
$1x10^{-5}$	64.2		3.2
$1x10^{-4}$	72.0		2.4
$1x10^{-3}$	77.4		1.9

Hydraulic gradients calculated below the base of the seepage barrier are presented in Table 4-16. In the cross section at Station 10+00 hydraulic gradients of up to 1.9 were calculated for seepage barriers with low hydraulic conductivity. In the cross section at Station 16+00 the calculated hydraulic gradients ware as high as 3.5. However, the higher gradients at this location are largely due to vertical seepage through the seepage blanket into the underlying embankment fill. While these gradients are relatively high, the erosion potential at the base of the barrier is likely low because the gradients are within clay material that is effectively filtered by the Lower Kirkwood Formation (at Station 10+00) or embankment fill (at Station 16+00).

Conclusions. Although the wide range of possible seepage barrier hydraulic conductivities prevent a precise assessment of the hydraulic conductivity, it is still possible to assess the maximum possible values. For the cross section at Station 10+00, the maximum hydraulic conductivity is about $1x10^{-6}$ cm/sec and at Station 16+00, the maximum is about $1x10^{-5}$ cm/sec. Thus, in the worst case, some of the hydraulic conductivity values may be up to an order of magnitude higher than the specified minimum of $1x10^{-6}$ cm/sec, and it is likely that the entire barrier has an effective hydraulic conductivity less than the specified maximum. Analyses using lower values were shown to also result in a seepage regime similar to that measured in the field. Thus, regardless of the actual hydraulic conductivity value, the analyses indicate that the seepage barrier is behaving in a manner consistent with the design intent.

Analyses on the Effects of Cracks on Barrier Performance

Finite element seepage analyses were performed on a simplified model to investigate the effects of three variables, (1) the aperture of a crack through a seepage barrier, (2) the hydraulic conductivity of the surrounding soil, and (3) the differential head across the barrier, on the effective hydraulic conductivity of the seepage barrier and the velocity of the water seeping through the crack.

Analyses. The analyses were performed on the simple two-dimensional finite element model shown in Figure 4-10. The model consists of a five-foot thick by 60-foot long layer of permeable soil with a two-foot thick seepage barrier located in the center. The top and bottom boundaries of the model are no-flow boundaries and the ends of the model are constant head boundaries. The analyses were performed using the computer program Phase2 (Rocscience 2007).

The analyses were performed in two stages that model a cracked seepage barrier and an intact seepage barrier as shown in Figure 4-11. The results of the analyses are representative of a single crack coinciding with a five-foot thick permeable layer, or repeated cracks spaced at five-foot intervals in a thicker layer. In the first case analyzed the seepage barrier was modeled with a crack at mid-height, and in the second case the

barrier was modeled with a constant hydraulic conductivity value to determine the "effective hydraulic conductivity" of the barrier. The procedure for modeling the crack in the barrier is discussed below. After each trial run on the model, the total seepage flows through the model in the two cases were compared, and the effective hydraulic conductivity for the second case was adjusted in successive runs until the total seepage flows for the two cases matched.

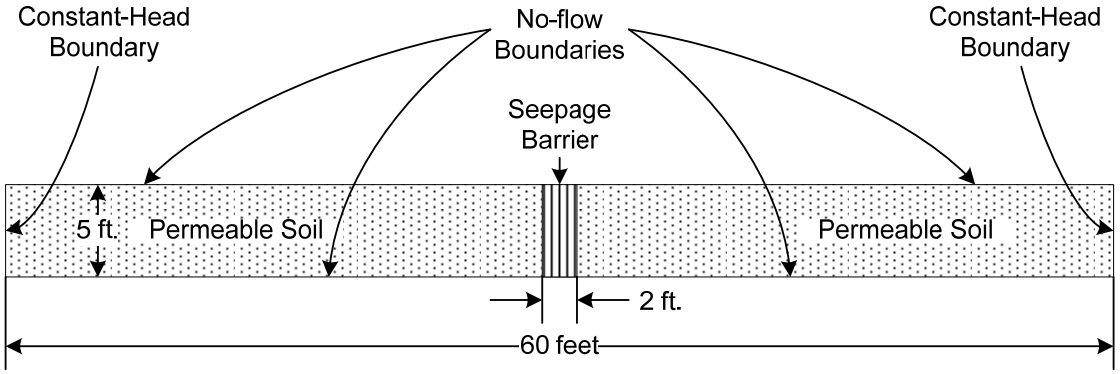

Figure 4-10 Two-dimensional finite element model for analyzing the effects of cracks in seepage barriers

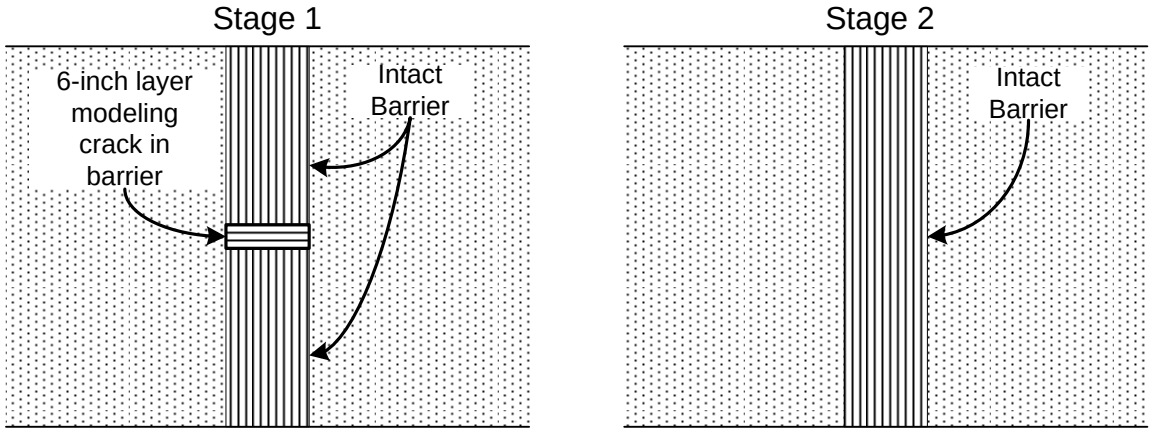

Figure 4-11 Details of the seepage barrier portion of the finite element model for Stages 1 and 2

The cracks in the seepage barrier were modeled using a six-inch high, horizontal layer through the seepage barrier that had a transmissivity equal to an equivalent-sized layer of the barrier with a crack at mid-height. The transmissivity of the crack was estimated using the Hagan-Poisuille equation (also referred to as the "cubic equation") based on the

assumed aperture of the crack. The Hagan-Poisuille Equation calculates the conductance, c, through a crack of constant aperture, e, and length, L, as follows:

$$c = \frac{g\, e^3}{12\, \nu\, L} \qquad 4\text{-}2$$

Where g is the gravitational acceleration (9.81 m/s^2), and ν is the kinetic viscosity of water (assumed to be $1x10^{-6}$ m^2/s for water). The transmissivity, T, is the conductance divided by the length of the crack, or:

$$c = \frac{T}{L} \qquad 4\text{-}3$$

Combining Equations 4-2 and 4-3 results in the transmissivity in terms of the crack aperture as follows:

$$T = \frac{g\, e^3}{12\, \nu} \qquad 4\text{-}4$$

The transmissivity through a soil layer of constant hydraulic conductivity, k, and constant thickness, b, is given by the equation:

$$T = k\, b \qquad 4\text{-}5$$

Assuming that the flow through the soil layer is predominantly through the crack, the equation for equivalent hydraulic conductivity, k_{eq}, through the six-inch layer is obtained by combining Equations 4-4 and 4-5 or:

$$k_{eq} = \frac{g\, e^3}{12\, \nu\, b} \qquad 4\text{-}6$$

Equivalent hydraulic conductivities calculated using Equation 4-6 for a six-inch layer with crack widths ranging from 0.1 mm to 4mm are presented in Table 4-17.

The Hagan-Poisuille Equation assumes a planar crack of constant aperture with smooth sides. While this may be representative of some joints between seepage barrier panels or horizontal cracks in soil-cement or jet-grout seepage barriers, it is not likely to be representative of cracks in concrete seepage barriers that are expected to have irregular crack sides. The irregular crack edges are expected to reduce the conductivity along the crack due to increasing the seepage length and adding tortuosity to the flow path. Therefore, the equivalent hydraulic conductivities presented in Table 4-17 would actually

represent a somewhat wider crack in a concrete seepage barrier. Because it is not the intent of these analyses to model specific cracks in barriers, it will suffice to say that the apertures presented in Table 4-17 should be considered to represent a relative level of crack transmissivity with the understanding that the actual width of the cracks may vary based on other factors.

Table 4-17 Calculated equivalent six-inch layer hydraulic conductivities representing crack apertures ranging from 0.1 to 4mm (calculated using Equation 4-6)

Crack Aperture (mm)	Equivalent Hydraulic Conductivity for six-inch layer, k_{eq} (cm/s)
0.1	0.00053
0.25	0.0082
0.5	0.066
0.75	0.22
1.0	0.52
2.0	4.2
4.0	34

Using the above described model, analyses were performed using differential total piezometric heads across the model of 20 feet and hydraulic conductivities of the permeable five-foot thick layer of $1x10^{-1}$, $1x10^{-2}$, and $1x10^{-3}$ cm/s. For each model run, the effective hydraulic conductivity of the seepage barrier corresponding to the flow through the cracked barrier was calculated along with the flow through the barrier and the velocity of the seepage through the barrier. The results of these analyses are presented in Table 4-18. Plots of the effective hydraulic conductivity versus crack aperture are shown in Figure 4-12, and plots of the velocity of the water seeping through the cracks versus crack aperture are shown in Figure 4-13.

Conclusions. The results of these analyses indicate that cracks with relatively small apertures can have a large effect on the effective hydraulic conductivity of the seepage barrier. A similar pattern resulted from the analyses for all cases of head and soil hydraulic conductivity values. As shown on Figure 4-12, the effective hydraulic conductivity of the seepage barrier increases with increasing crack aperture when the aperture is relatively small and then plateaus at a near-constant value that is not

significantly affected by further increases in the aperture. Below the plateau, the amount of flow through the crack is controlled by the hydraulic conductance through the crack. The plateau area corresponds to the conditions where the flow through the crack is controlled by the soil surrounding the entrance and exit of the crack. As the hydraulic conductivity of the soil is increased, the breaks in the curves occur at higher values of crack aperture indicating more water is being allowed to flow to the crack entrance.

As shown in Figure 4-13, the velocity of the water seeping through a crack will increase with increasing aperture for small crack apertures and then decrease as the aperture continues to increase. The decrease in flow velocity is due to the flow volume becoming controlled by the flow though the soil at the crack inlet and outlet. Therefore, as a crack in a seepage barrier widens, the seepage velocity in the crack will initially increase and then decrease.

Table 4-18 Results of seepage barrier crack finite element analyses

Soil Hydraulic Conductivity (cm/s)	Crack Aperture (mm)	Equivalent Hydraulic Conductivity of Seepage Barrier (cm/s)	Flow through Crack (ft^3/s)	Velocity in Crack (ft/s)
$1x10^{-1}$	0.1	0.000051	0.000083	0.25
	0.25	0.00076	0.0010	1.23
	0.5	0.0042	0.0029	1.79
	0.75	0.0078	0.0036	1.47
	1.0	0.0096	0.0038	1.16
	2.0	0.012	0.0040	0.61
	4.0	0.012	0.0040	0.24
$1x10^{-2}$	0.1	0.000049	0.00037	0.21
	0.25	0.00048	0.0016	0.37
	0.5	0.0010	0.0020	0.23
	0.75	0.0012	0.0023	0.16
	1.0	0.0012	0.0023	0.12
	4.0	0.0012	0.0023	0.024
$1x10^{-3}$	0.1	0.000036	0.00014	0.083
	0.25	0.00010	0.00020	0.047
	0.5	0.00012	0.00021	0.024
	0.75	0.00012	0.00021	0.016
	1.0	0.00012	0.00021	0.012
	4.0	0.00012	0.00021	0.0024

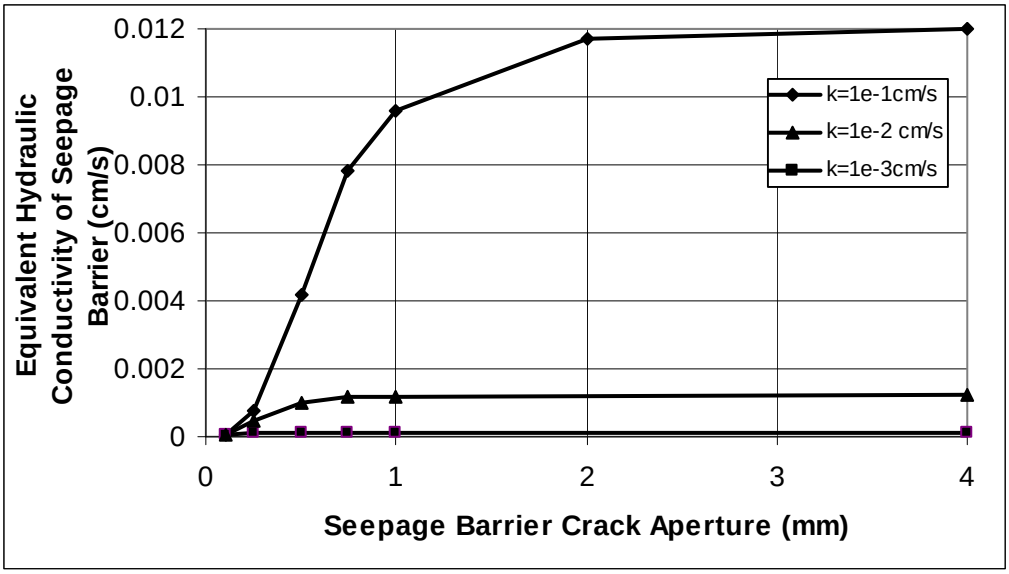

Figure 4-12 Plot of calculated equivalent hydraulic conductivity for cracked barrier versus the aperture of the crack

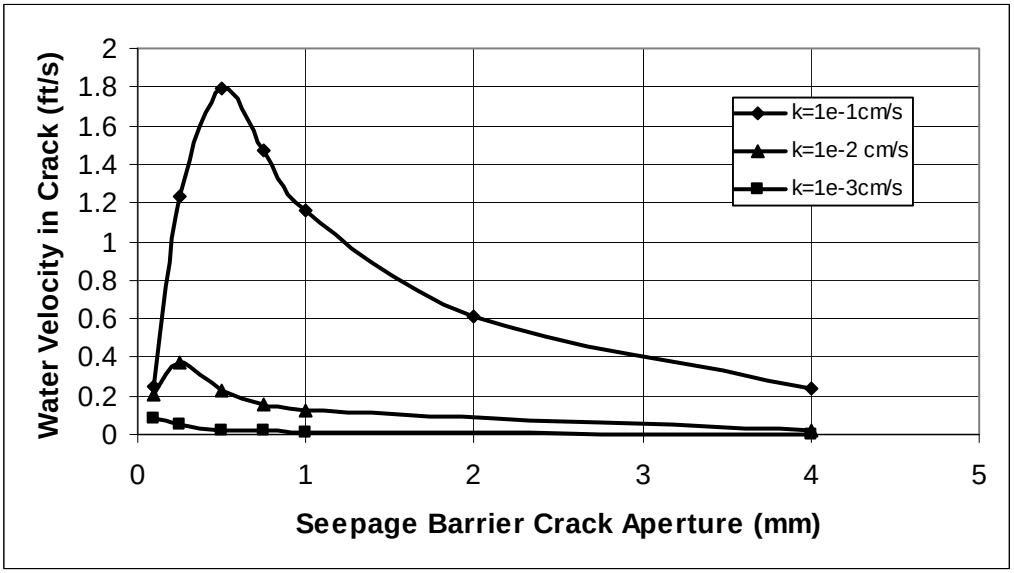

Figure 4-13 Plot of calculated seepage water velocity in a crack in a seepage barrier versus the aperture of the crack

The consequences for long-term seepage barrier performance indicated by the results of these analyses are two-fold. First, the analyses indicate that cracks with small apertures can have a significant affect on the effective hydraulic conductivity of the barrier, and

second, as cracks widen, the susceptibly of the seepage barrier infill to erosion decreases due to decreasing water velocity in the crack.

Cracks with apertures less than a millimeter in a five-foot soil layer can increase the effective hydraulic conductivity of the barrier by nearly four orders of magnitude. The percentage increase in effective hydraulic conductivity due to a crack will be less if it is located in a thicker permeable soil layer. At a moderate crack aperture, the effect of the crack does not increase as the crack widens due to the flow being controlled by the soil at the entrance and exit points of the crack. However, if soil erosion takes place at the entrance or exit points of the crack, resulting in a void or a pocket of high-permeability soil, the amount of water entering the crack, and consequently the effect on effective hydraulic conductivity, will continue to increase.

Assuming no soil erosion takes place at the crack entrance and exit points, the relationship between crack aperture and water velocity in the crack indicates that, even if the velocities of the water in the crack are initially high enough to erode the seepage barrier material, the velocities will decrease as the erosion progresses and will eventually reach a level that is no longer erosive to the barrier material. However, similar to the case with effective hydraulic conductivity, if erosion of the soil does occur, the water velocity in the crack can continue to increase and with it, the crack erosion potential.

The above discussion indicates that the factors controlling whether a crack in a seepage barrier will enlarge due to erosion are the resistance of the seepage barrier backfill to erosion and the tendency of the surrounding soil to erode at the crack entrance and exit points. The erosivity of the barrier backfill is a function of the type of backfill and the cement content and should be assessed on an individual basis. Because very high hydraulic gradients are expected at the entrance and exit points of a crack, the potential for erosion at these locations is contingent on the ability of the eroding soil particles to be removed from the area surrounding the crack. At the crack entrance, the eroded soil particles would need to travel through the crack and away from the exit point. Based on the Hazen Equation (Freeze and Cherry 1979), a very simple relationship between

hydraulic conductivity and soil gradation, the D_{10} of the soil in millimeters is approximately equal to the square root of the hydraulic conductivity in centimeters per second. The estimated D_{10} corresponding to the three hydraulic conductivity values used in the analyses are presented in Table 4-19. Comparison of the D_{10} values in Table 4-19 with Figure 4-13 indicates that the D_{10}-sized particles are smaller than the crack apertures where the maximum water velocities were calculated for the respective hydraulic conductivity values. Therefore, depending on the gradation of the soil, it appears possible that erosion of at least the fine portion of the soil through the crack is possible. The controlling factor then appears to be the ability of eroded soil particles to be removed from the area around the crack exit point. Such removal of particles is possible if the crack is located near bedrock with open joints or a layer of open graded gravel. Eroded particles may also be removed if the eroding soil is not self filtering (a gap graded soil for instance) and the particles can move through the soil matrix (a process often referred to as suffusion).

Table 4-19 Estimated D_{10} of soil corresponding to the hydraulic conductivities of soils used in the crack effect analysis

Hydraulic Conductivity (cm/s)	Estimated D_{10} of Soil Based on Hazen Equation (mm)	Crack Aperture where Peak Velocity Calculated (mm)
$1x10^{-1}$	0.3	0.5
$1x10^{-2}$	0.1	0.25
$1x10^{-3}$	0.03	<0.1

Summary of Insights from Analyses

The following sections present insights regarding the performance of seepage barriers that were garnered from the results of the analyses discussed above. The insights are presented under the headings of:

- Effective Hydraulic Conductivity,
- Reduction of Exit Gradients,
- Hydraulic Gradients Developed Below Seepage Barriers,

- Hydraulic Gradients and Differential Heads Developed Across Seepage Barriers,
- Seepage Barrier Deformation and Cracking, and
- Consequences of Seepage Barrier Cracking.

Effective Hydraulic Conductivity

The effective hydraulic conductivities of the seepage barriers were calculated for six cross sections of Upper and Lower Clemson Dams, one cross section at Wister Dam, one cross section at Virginia Smith Dam, and two cross sections at Manasquan Dam. The results of these analyses are summarized in Table 4-20. While seepage analyses were performed on Fontenelle and Navajo Dams, the high hydraulic conductivity of the bedrock combined with the configurations of these dams made assessing the effective hydraulic conductivity with a useful level of precision difficult.

Table 4-20 Calculated values of effective hydraulic conductivity of seepage barriers

Dam	Barrier Type	Range of Effective Hydraulic Conductivity	
		High	Low
Upper Clemson	Concrete	3.0×10^{-5}	6.1×10^{-6}
Lower Clemson	Concrete	1.1×10^{-4}	4.7×10^{-5}
Wister	Plastic Concrete	2.0×10^{-5}	2.0×10^{-6}
Virginia Smith	Soil-Bentonite	1.7×10^{-5}	1.7×10^{-6}
Manasquan	Soil-Bentonite	1.0×10^{-5}	1.0×10^{-7}

The seepage analyses performed on Virginia Smith and Manasquan Dams indicated that order of magnitude changes in the effective hydraulic conductivity of the seepage barrier had small effects on the calculated water pressure regimes. Therefore, the ranges of effective hydraulic conductivity presented for these dams in Table 4-20 are representative of the relatively low level of precision that the models from these dams are able to back calculate effective hydraulic conductivity with. This differs from the analyses performed on Upper Clemson, Lower Clemson, and Wister Dams where relatively small changes in the effective permeability had a significant effect on the calculated seepage regime. Therefore, the ranges of effective hydraulic conductivity presented for these dams

represent ranges of more precisely calculated values calculated for several different sections of the dams.

The difference in the level of precision obtained is largely associated with the thickness of downstream permeable layers. For example, the permeable layer in Manasquan Dam is the embankment material, and any amount of water seeping through the embankment is quickly drained so that the downstream piezometric heads are not sensitive to the quantity of seepage through the barrier. In contrast, the most permeable layers in Upper and Lower Clemson Dams are relatively thin, confined layers in the alluvium. Thus smaller changes in the quantity of seepage through the barrier have a significant effect on the downstream pore pressure regime.

The high effective hydraulic conductivities calculated in the barriers in Upper and Lower Clemson Dams and Wister Dam are likely due to two factors: (1) cracking of the barriers, and (2) seepage through bedrock joints beneath the barrier. As discussed below, the deformation analyses performed on these dams indicated that the differential water pressure across the barrier is likely to cause deformations of the barrier large enough to induce cracking of the barrier. The analyses on the effects of cracks on seepage barriers indicated that cracks with apertures of less than a millimeter can increase the effective hydraulic conductivity of a barrier by as much as six orders of magnitude. Therefore, it can be concluded that cracking of the barrier can account for the values of effective hydraulic conductivity calculated for these dams. Down-hole permeability tests (slug tests) performed during the investigations for these dams identified zones where very high flows were encountered within the generally tight bedrock in the dam foundations. While it is difficult to quantify and analyze the effects of these zones, it appears feasible that flow through such zones may also contribute to the high effective hydraulic conductivity calculated in these seepage barriers.

The range of calculated effective hydraulic conductivity values for Virginia Smith and Manasquan Dams are not much different from their design hydraulic conductivity values. It should be noted that both soil-bentonite barriers are embedded in either clay or tight

sandstone/claystone bedrock, while the three rigid barriers are embedded in bedrock containing significant jointing. These conditions at the base of the barrier likely contribute, to some degree, to the high effective hydraulic conductivities calculated for the rigid barrier types. However, the performance of the soil-bentonite barriers may also indicate that their ductility prevents the development of cracking and, thus the equivalent hydraulic conductivities are closer to the hydraulic conductivities of the backfill material.

Reduction of Exit Gradients

The change in exit gradient due to the construction of the seepage barrier was calculated for Upper and Lower Clemson Dams and Wister Dam. In Navajo and Fontenelle Dams, the erosion mechanism of concern that prompted the seepage barrier construction was internal erosion along bedrock joints and, consequently, exit gradients were not a concern. The seepage barriers in Virginia Smith and Manasquan Dams were built in the original construction and no comparison can be made with a pre-barrier condition.

The analyses showed that the exit gradients at Upper and Lower Clemson Dams were reduced by 50 to 70 percent with the construction of the seepage barrier. At Wister Dam, the analyses indicate no significant change in the already low exit gradients (existing exit gradients of about 0.1). These results indicate that, where high exit gradients exist, the seepage barrier is effective in reducing the gradient, even if the effective hydraulic conductivity of the barrier is several orders of magnitude higher than the design. The effectiveness in reducing exit gradients is due to the ability of the seepage barrier, even with hydraulic conductivity much greater than intended, is able to reduce the flow volume through the dam by several orders of magnitude. This reduction in flow is responsible for reducing the exit gradients.

Hydraulic Gradients Developed Below Seepage Barriers

The ranges of hydraulic gradients calculated in the soil or rock beneath the bases of the seepage barriers are presented in Table 4-21. The calculated hydraulic gradient values

range from 1.1 to 5.2, all of which could be considered erosive to soils if not protected by effective filtering. Based on the analyses, the magnitude of the hydraulic gradients is a function of the following: (1) the differential hydraulic head across the barrier, (2) the depth of embedment into a low permeability layer, (3) the ratio of hydraulic conductivities of the permeable layer being cut off and the low permeability layer, (4) the configuration of the seepage barrier and other soil layers in the dam cross section. The effects these factors have on the magnitude of the hydraulic gradient for the subject dams are discussed below.

Table 4-21 Range of calculated hydraulic gradients below the seepage barrier

Dam	Calculated Hydraulic Gradient Below the Seepage Barrier(cm/s)	
	High	Low
Upper Clemson	1.7	1.9
Lower Clemson	1.4	1.9
Wister	3.7	1.6
Fontenelle	4.8	4.8
Navajo	1.1	1.1
Virginia Smith	5.2	1.2
Manasquan	3.5	1.9

In Upper and Lower Clemson Dams and Wister Dam the moderate hydraulic gradients calculated are largely due to the relatively low differential hydraulic head across the barrier (ranging from 17 to 27 feet). Similarly designed barriers in higher dams or dams where the barriers have higher head efficiencies would result in proportionally higher hydraulic gradients. The gradients in Upper and Lower Clemson Dams are imposed on joints and shear zones in the granitic bedrock and, based on the good long-term performance of the barriers, do not appear to be eroding significant amounts of soil. Therefore, it can be concluded that the material in the joints and shear zones is either not erodible or the eroding particles are effectively filtered by the overlying alluvial soil. In Wister Dam, there is evidence that the increased hydraulic gradient may be acting to erode bedrock joint infill in the sandstone and shale foundation. However, this process, if occurring, is localized and has a small effect on the overall dam performance.

Fontenelle and Navajo Dams have similar embankment and foundation conditions, yet, although Navajo Dam has a much higher differential hydraulic head across the dam, the calculated hydraulic gradients below the seepage barrier are much lower than in the foundation. The lower hydraulic gradients in Navajo Dam are the result of the deep embedment of the seepage barrier into the foundation bedrock. It should also be noted that the calculated hydraulic gradients assume homogeneous hydraulic conductivity values in the bedrock masses. In actuality, the flow through bedrock is concentrated in the joints and will have considerably higher velocities than calculated using the homogeneous model. This will result in much higher erosion potential for any soil or soft rock in or adjacent to the bedrock joints. In both Fontenelle and Navajo Dams, there is evidence of decreasing seepage resistance in the bedrock below or around the seepage barriers. While this data does not appear to represent a substantial risk to the dams, it is evidence of an erosion mechanism acting in areas where high hydraulic gradients have developed around or below seepage barriers.

The wide range of calculated hydraulic gradients in Virginia Smith and Manasquan Dams are due to considerable differences between the configurations of the dam and seepage barrier in the cross sections analyzed. The higher hydraulic gradient was calculated in Virginia Smith Dam where the seepage barrier completely penetrated the permeable layers and was embedded into low-permeability bedrock, and the lower gradients were calculated where the barrier partially penetrated the permeable layer. In Manasquan Dam, the lower hydraulic gradient was calculated where the bottom of the barrier was embedded in a thick clay layer and the higher gradient calculated where the barrier was embedded in a thin clay layer underlain with permeable soil, thus adding a vertical component to the hydraulic gradient. In both dams the high hydraulic gradients were calculated within low permeability soil or bedrock layers that are adjacent to soils that act as effective filters should erosion initiate due to the gradients.

The above discussion illustrates that the magnitude of hydraulic gradient that develops at the base of a seepage barrier is a function of multiple factors. As a result, it is important to analyze each dam and seepage barrier individually to assess the potential for

developing high hydraulic gradients. Once the hydraulic gradient has been analyzed, an assessment can be made to assess the potential for high gradients to cause internal erosion. Such an assessment should look at the erodibility of the soils subject to high hydraulic gradients and velocities and the presence of a pathway for removal of eroded soil particles. The effectiveness of adjacent soils and rock formations as a filtering mechanism for the eroding soil particles should also be assessed.

Hydraulic Gradients and Differential Heads Developed Across the Seepage Barrier

The hydraulic gradients and differential hydraulic heads calculated across the seepage barriers are presented in Table 4-22. Hydraulic gradients ranging from 8 to 47 and differential hydraulic heads ranging from 18 feet to 166 feet were calculated across the barriers. The significance of the hydraulic gradients is that when a crack or other defect exists in the barrier the water flowing through the defect will be driven by the very high gradient and have the potential to be highly erosive to the soils and or seepage barrier. The behavior of water flowing through cracks was analyzed with seepage analyses and is discussed further below.

Table 4-22 Hydraulic gradients and differential hydraulic heads calculated across seepage barriers

Dam	Maximum Calculated Hydraulic Gradient Across the Seepage Barrier (cm/s)	Maximum Calculated Differential Head Across the Seepage Barrier (ft.)
Upper Clemson	11	23
Lower Clemson	13	27
Wister	9	18
Fontenelle	26	52
Navajo	47	166
Virginia Smith	8	40
Manasquan	8	41

The significance of the differential head across the barrier is that it concentrates seepage forces at the barrier location that would have been distributed across the embankment without the barrier in place. These concentrated seepage forces result in deformation of the barrier that can cause cracking of rigid barriers.

Seepage Barrier Deformation and Cracking

Deformation analyses were performed for five dams having rigid seepage barriers: Upper and Lower Clemson, Wister, Fontenelle, and Navajo. A summary of the results of these analyses is presented in Table 4-23. In all of the cases analyzed the deformation of the barriers caused bending moments large enough to result in tensile stresses close to or greater than the estimated tensile strength of the barriers. In all of the cases, the maximum moment was developed at or near the interface between the alluvium and the bedrock or the base of the embankment and the bedrock. Thus, it is likely that all of the barriers analyzed have cracked due to deformation caused by the concentration of seepage forces and the most likely location for this cracking is at the base of the alluvium or at the interface between the embankment and the bedrock.

Table 2-23 Summary of results of seepage barrier deformation analyses

Dam	Maximum Horizontal Deflection of Seepage Barrier (in)	Tensile Stresses in Seepage Barrier Due to Bending Moment (percentage of estimated tensile strength of barrier)
Upper Clemson	0.3	108
Lower Clemson	0.3	91
Wister	0.4	117
Fontenelle	1.1	188
Navajo	7.7	715

At Navaho Dam, cores were drilled into the seepage barrier to check for crack locations. Cracks were located at the interface between the embankment and the bedrock in about half of these cores. Cracks were also detected in locations well within the embankment and well within the bedrock. The cracks located within the bedrock appear to be aligned along bedding planes between sandstone and shale layers and are thought to be due to moments caused by the different amounts of deflection in the sandstone and shale layers, due to the different stiffnesses of the rock types. The cracks detected within the embankment may be due to shrinkage or thermal cracking.

Consequences of Seepage Barrier Cracking

Analyses were performed to assess the effects of cracking on the performance of seepage barriers. The analyses indicate that cracks with apertures of less than one millimeter can have a significant effect on the effective hydraulic conductivity of the barrier. Therefore, it is possible that the high effective conductivities that were calculated for the rigid seepage barriers are the result of barrier cracking due to deflection or other mechanisms.

Another effect of seepage barrier cracking is groundwater flow under very high hydraulic gradients through the seepage barrier and in the soils near the entrance and exit points of the crack. The analyses showed that the seepage velocity in the crack would decrease as the crack widened. As a result, if a crack begins to enlarge due to erosion from high velocity seepage, the potential for erosion of the barrier infill will decrease as the crack widens. On the other hand, if there is erosion of the soil near the ends of the crack, the erosion will result in more water being allowed to enter the crack, thus allowing the seepage velocity in the crack to be maintained or increase.

Because a high hydraulic gradient is expected near most cracks that occur through seepage barriers, whether or not erosion of the soil near the ends of a crack occurs will depend on whether or not there is a pathway for the removal of the eroding soil particles. Two possible types of pathways are open bedrock joints and open-graded or gap-graded gravelly soils. As evidenced in many of the dam foundation case studies, gravelly soils often occur at the base of fluvial soil deposits. Therefore, both of the scenarios for pathways to remove eroding soil particles occur at the base of the alluvium layer where the potential for developing cracks in the seepage barrier is largest.